



Published in final edited form as:

Nat Chem Biol. 2022 November ; 18(11): 1277–1286. doi:10.1038/s41589-022-01138-9.

Context-based sensing of orthosomycin antibiotics by the translating ribosome

Kyle Mangano^{1,2,†}, James Marks^{1,2,††}, Dorota Klepacki^{1,2}, Chayan Kumar Saha^{3,4}, Gemma C. Atkinson³, Nora Vázquez-Laslop^{1,2,*}, Alexander S. Mankin^{1,2,*}

¹Center for Biomolecular Sciences, University of Illinois at Chicago, Chicago, IL 60607, USA

²Department of Pharmaceutical Sciences, University of Illinois at Chicago, Chicago, IL 60607, USA

³Department of Experimental Medicine, Lund University, 221 84 Lund, Sweden

⁴Department of Molecular Biology, Umeå University, 901 87 Umeå, Sweden

Abstract

Orthosomycin antibiotics inhibit protein synthesis by binding to the large ribosomal subunit in the tRNA accommodation corridor which is traversed by incoming aminoacyl-tRNAs. Structural and biochemical studies suggested that orthosomycins block accommodation of any aminoacyl-tRNAs in the ribosomal A-site. However, the mode of action of orthosomycins in vivo remained unknown. Here, by carrying out genome-wide analysis of antibiotic action in bacterial cells, we discovered that orthosomycins primarily inhibit the ribosomes engaged in translation of specific amino acid sequences. Our results reveal that the predominant sites of orthosomycin-induced translation arrest are defined by the nature of the incoming aminoacyl-tRNA and likely by the identity of the two C-terminal amino acid residues of the nascent protein. We show that nature exploits this antibiotic-sensing mechanism for directing programmed ribosome stalling within the regulatory open reading frame that may control expression of an orthosomycin resistance gene in a variety of bacterial species.

*Corresponding authors: Nora Vázquez-Laslop (nvazquez@uic.edu), Alexander Mankin (shura@uic.edu). *Editorial correspondence:* Alexander S. Mankin, Center for Biomolecular Sciences – m/c 870, University of Illinois at Chicago, 900 S. Ashland Ave., Rm. 3056, Chicago, IL 60607, shura@uic.edu.

†Present address: Amgen Research, Thousand Oaks, CA 91320, USA

††Present address: National Institute of Arthritis and Musculoskeletal and Skin Disease (NIAMS), Bethesda, MD 20894, USA

Authors contributions

K.M., J.M., N. V.-L. and A.S.M. designed research. D. K. carried out Ribo-seq experiments, *emtA* induction studies, and some toeprinting experiments. J.M. performed the initial analysis of the Ribo-seq data. K.M. carried out comprehensive analysis of the Ribo-seq data, performed the majority of the toeprinting experiments and analyzed inducibility of the *emtA* gene. C.K.S. and G.C.A. analyzed conservation of the EmtA methyltransferase, phylogenetic distribution of the *emtA* genes, and conservation of the *emtAL* ORF. K.M., J.M., G.C.A., N. V.-L. and A.S.M. analyzed data; K.M, N.V.-L. and A.S.M. wrote the manuscript.

Competing interests

The authors declare no competing interests

Code availability

The scripts for Ribo-seq analysis can be found at the following link: <https://github.com/mmaienc/RiboSeq>. The metagenome analysis custom scripts are available at <https://github.com/adamhockenberry/ribo-t-sequencing>. The eUIgene.py Python script is available at <https://github.com/GCA-VH-lab/eUIgene>.

Keywords

ribosome; antibiotics; context-specificity; nascent peptide; aminoacyl-tRNA; orthosomycin

Introduction

Orthosomycins (OSMs) are oligosaccharide antibiotics that inhibit bacterial growth by interfering with protein synthesis (reviewed in ref.¹). The most extensively studied OSMs are avilamycin (AVI), used in veterinary medicine, and evernimicin (**1**) (EVN) (Fig. 1a), which shows good activity against several Gram-positive human pathogens, including streptococcal, staphylococcal and enterococcal strains¹. With the growing problem of multi-drug resistance pathogens, OSMs remain highly attractive due to their unusual mechanism of action and the lack of cross-resistance with other antibiotics.

OSMs inhibit bacterial protein synthesis by interacting with the large (50S) subunit of the bacterial (but not eukaryotic) ribosome². Most of the antibiotics targeting the 50S subunit bind either at the peptidyl transferase center (PTC) or the nascent peptide exit tunnel (NPET)³. In contrast, OSMs interact with a site located in the aminoacyl-tRNA (aa-tRNA) accommodation corridor, a groove in the 50S subunit that is navigated by aa-tRNA on its way to the PTC A site after the codon-anticodon interactions have been established in the decoding center of the small subunit⁴⁻⁷. Bound at this unique location, OSMs inhibit protein synthesis via a distinct mechanism which has not been fully elucidated.

Although the effects of OSMs on translation have been examined in several in vitro studies, it is difficult to reconcile the available data into a consistent model. EVN was reported to impair IF2-dependent formation of the 70S initiation complex^{5,8} and some toeprinting experiments, which map the location of stalled ribosomes on mRNA, suggested that the drug causes arrest at start codons⁷. However, EVN also inhibits translation of poly(U) or poly(A) homopolymers which does not rely on canonical IF2-dependent initiation^{2,9}. Other biochemical studies suggested that EVN interferes with the activities of EF4 (LepA) and BipA⁸, two enigmatic proteins involved in translation and ribosome assembly^{10,11}. Consistent with the location of the EVN binding site in the accommodation corridor^{6,7}, single-molecule fluorescence resonance energy transfer (smFRET) studies showed that EVN hinders the stable placement of aa-tRNA in the A site^{7,12}. The smFRET results, buttressed by structural studies, implied that EVN may act as an indiscriminate obstacle of every elongation step because any aa-tRNA is expected to clash with the drug at the accommodation corridor. Nevertheless, it has been shown that EVN arrests ribosomes during in vitro translation only at specific codons within ORFs¹³, suggesting that the antibiotic action may depend on the nature of the mRNA, tRNA, donor or acceptor amino acid, or the nascent polypeptide.

While highly informative, in vitro approaches are carried out in dramatically simplified settings where ribosomes translate only one mRNA and, therefore, they provide limited insights on the genome-wide effects of translation inhibitors. To overcome these limitations and characterize the action of OSM antibiotics in bacterial cells we used ribosome profiling (Ribo-seq), a technique which monitors progression of the ribosomes through translated

mRNAs^{14,15} and provides a global view of how an antibiotic inhibits translation of every expressed gene^{16,17} (reviewed in¹⁸). Our Ribo-seq results, supported by biochemical experiments, show that the OSM antibiotic EVN stalls ribosomes attempting to polymerize specific amino acid sequences. We further show that the context-specificity of EVN action is exploited for sensing the presence of antibiotic and activating the expression of OSM-resistance genes via programmed translation arrest within the regulatory leader open reading frame (ORF).

Results

EVN in vitro effects differ between individual genes

Using in vitro toeprinting analysis to define the mechanism of EVN action, one study showed EVN-mediated ribosomes stalling at the start codon of the *Escherichia coli hns* gene⁷ while another report found ribosomes arrested by the drug at a specific internal codon of *ermBL*¹³. Given those seemingly conflicting results, we compared the effect of the drug upon progression of the ribosome along individual ORFs in a side-by-side toeprinting experiment (Fig. 1b and Extended Data Fig. 1a). While we could reproduce the reported drug-induced arrest at the start codon of *hns* (Extended Data Fig. 1a), in most of the other tested templates EVN interrupted translation at a variety of discrete positions within the ORFs.

To test whether EVN also acts in vivo primarily as inhibitor of translation elongation rather than initiation, as suggested by our toeprinting results, we analyzed polysomes isolated from OSM-sensitive *E. coli* cells¹⁹ exposed to the antibiotic (Extended Data Fig. 2). An initiation inhibitor would cause the elongating ribosomes to run off the mRNAs and polysomes would be converted into monosomes or unassociated ribosomal subunits²⁰. However, neither a prolonged (30 min) exposure of cells to 1x the EVN minimal inhibitory concentration (MIC), nor a shorter (4 min) treatment with 100x MIC of the drug led to significant decomposition of polysomes or accumulation of free subunits, indicating that EVN likely interferes with translation elongation in bacterial cells.

Genome-wide analysis of EVN action in bacterial cells

To unravel the specificity of EVN action in the cell, we performed Ribo-seq experiments with *E. coli* cells treated for 4 min with 100x MIC of EVN – conditions resulting in a nearly complete cessation of protein synthesis (Extended Data Fig. 3a–c).

If the effect of EVN in the cell is to preferentially arrest initiating ribosomes or abolish binding of the first elongator aa-tRNA, the antibiotic treatment should lead to the appearance of a characteristic sharp peak of increased ribosome occupancy of the genes' start codons^{20,21}. Alternatively, if EVN acts as a universal inhibitor of aa-tRNA accommodation, as proposed by some studies^{7,8}, ribosomes should 'freeze' at every act of elongation, thus preserving the ribosomal footprints (rfps) distribution through the entire gene as observed in the untreated control. However, the metagene analysis of the rfp density in the vicinity of the start codons did not conform to either of these scenarios. Instead, we observed a general preservation of rfp density along the ORFs accompanied by a global overall increased

ribosome occupancy at the first ~20 codons (Fig. 1c). The increased occupancy of the early codons can be attributed to ribosomes initiating new rounds of translation after the antibiotic addition and then becoming arrested at specific sites proximal to the start codons of the ORFs. A similar trend was noted previously in Ribo-seq analysis of cells treated with macrolide antibiotics¹⁷, or upon deletion of the yeast elongation factor eIF5A²², conditions that cause ribosome arrest at specific gene locations.

The A-site codon-anticodon interactions influence EVN action

In agreement with the notion that EVN may be a context-specific elongation inhibitor, we observed a significant redistribution of rfps along individual ORFs in EVN-treated cells compared to the untreated control, with peaks of varying intensity appearing throughout the ORFs (Fig. 1d, Extended Data Fig. 4). This pattern suggested that EVN exhibits stronger action at particular sites while allowing fairly unimpeded translation of other mRNA sequences. Therefore, we sought to identify the features of the predominant sites of EVN action.

Because EVN binds in the aa-tRNA accommodation corridor^{6,7}, we reasoned that the drug action could be influenced by the features of the incoming aa-tRNAs. Therefore, we calculated a genome-wide EVN stall score for each of the 61 sense codons in the ribosomal A-site, a metric that reflects the codon occupancy change in EVN-exposed cells relative to the control. Indeed, this analysis showed that Leu and Pro (and to a lesser extent, His and Gln) codons were enriched in the A site of the EVN-stalled ribosomes (Fig. 2a). In addition, distinct Arg, Ile and Gly codons were also associated with the preferential EVN translation arrest (Fig. 2a). The properties of the incoming aa-tRNAs decoding the A-site codons conducive to EVN action may affect the interaction of the tRNA with mRNA or with the ribosome-bound antibiotic. To distinguish between these possibilities, we explored EVN-dependent ribosome stalling at two different Arg codons, the non-stalling CGU and the strongly stalling CGA (Fig. 2a), decoded by the same tRNA_{2^{Arg}} with the anticodon ICG. Replacement of the Arg₇ CGU codon of *ermBL*, where EVN-bound ribosome does not stall, with the synonymous CGA codon resulted in the appearance of a new toeprint band (Fig. 2b), indicative of drug-induced ribosome arrest with the CGA codon in the A site. Because with both templates, the interaction of Arg-tRNA_{2^{Arg}} with EVN should remain unchanged, this result underscores the importance of the A-site codon-anticodon interactions in defining the sites of preferential EVN-induced arrest. This conclusion is further supported by the presence of idiosyncratic posttranscriptional modifications in the anticodon loops of several aa-tRNAs specifically associated with the preferential sites of EVN action (Fig. 2a) (see Discussion).

The sole identity of the A-site codon, however, is not sufficient to determine EVN-directed arrest because EVN-bound ribosomes encountering the same codon at different locations within an ORF may or may not stall (Extended Data Fig. 5a). We therefore reasoned that besides the nature of the A-site aa-tRNA, EVN action must be modulated by a more extended sequence context.

Sequence motifs at the sites of prevalent EVN action

We investigated whether particular amino acid sequences are encoded at the strongest EVN stalling mRNA sites (Fig. 2c,d). Consistent with the specific A-site codon preference previously identified (Fig. 2a), pLogo plots showed a significant overrepresentation of Leu or Pro as the acceptor substrates (position +1) at these sites (Fig. 2d). In addition, Pro residues were also overrepresented at the C-terminus (position 0) and as the penultimate amino acid (position -1) of the nascent chain (Fig. 2d). Because pLogo analysis reports on enrichment of residues at independent positions but not directly on their sequence, we calculated the EVN stall scores for all possible tripeptides with sufficient ribosome occupancy ($n=4047$) (Fig. 3a, Supplementary Dataset). Several motifs emerged from this analysis (Fig. 3a–b). Consistent with the pLogo plot (Fig. 2d), nearly 60% of the EVN-susceptible sequences include Pro residues at one or more of the -1, 0, or +1 positions. Over 25% of the tripeptides contain Leu at position +1 (motifs PXL, XPL and X,K/R/H,L), underscoring the finding of the A-site codon analysis that EVN more readily arrests ribosomes trying to accommodate Leu-tRNA (Fig. 2a). In addition, a sizable fraction (11%) of the EVN susceptible sequences conformed to the Arg/Lys – X – Arg/Lys consensus (Fig. 3b), a sequence that had been designated as the “+ X +” motif found at the sites of translation arrest induced by macrolide antibiotics^{16,17,23,24}. No common motifs were readily recognizable in some (14%) of the tripeptides (Fig. 3b, Supplementary Dataset).

We asked whether the identified tripeptide sequences would be sufficient to direct EVN-mediated translation arrest when placed in an ORF otherwise refractory to the drug action. To test this, we individually introduced EVN-susceptible tripeptides of the different categories to substitute the Val-Asp-Lys (V₉D₁₀K₁₁) sequence of *ermBL*, which is impervious to EVN arrest during in vitro translation (Fig. 3c). Toeprinting analysis demonstrated that grafting the sequences encoding the selected tripeptide motifs into *ermBL* was sufficient to direct EVN-dependent arrest at the engineered mRNA sites (Fig. 3c). Noteworthy, replacement of the wt ‘benign’ VDK sequence with the ‘problematic’ PLP and PPQ tripeptides allowed not only for EVN-mediated arrest at the predicted sites (Leu11 or Pro11 codons, respectively, of the modified *ermBL* templates, red arrows in Fig. 3c), but also at the preceding codon (pink arrows in Fig. 3c) because insertion of these tripeptides generated additional EVN stalling sequences, NPL and NPP, which conform to the XPL and the XPP motifs, respectively (Fig. 3b,c).

Altogether, our Ribo-seq data and in vitro experiments revealed that the action of EVN critically depends on specific codons within an ORF and likely on the sequence of the protein being translated.

Nascent peptide - aa-tRNA interplay influences EVN action

The occurrence of specific tripeptide motifs at the sites of EVN action suggests that not only the incoming aa-tRNA but also likely the C-terminal sequence of the growing protein chain contribute to stalling by EVN. We used toeprinting analysis to further dissect the context requirements for EVN action on the arrest observed in vivo at the PSP₁₁ sequence (the PXP motif) of the *gltX* gene (Fig. 3d). To facilitate such in vitro analysis, we introduced minor modifications into the *gltX* template (Extended Data Fig. 6a). In the reactions devoid of

EVN, ribosomes translate the modified *gltX* template up to the Trp₁₃ trap-codon (Fig. 3e, lane 1, white arrow). As expected, addition of EVN arrests ribosomes with the Ser₁₀ codon of the PSP₁₁ motif placed in the P site (Fig. 3e, lane 2, red arrow). Alanine scanning of the PSP₁₁ motif reduced efficiency of the drug action (Fig. 3e, lanes 3–5). Replacing Ser₁₀ of the motif with other amino acids had varying effects on stalling (Extended Data Fig. 6b), compatible with the possibility that the properties of the nascent protein C-terminus modulate EVN action. Finally, simultaneously changing any two or all three residues of the *gltX*PSP₁₁ sequence to alanines essentially eliminated the EVN-mediated translation arrest (Fig. 3e, lanes 6–10).

An alternative possibility to explain the conservation of tripeptide motifs at the sites of EVN action could be related to the presence of specific tRNAs in the ribosomal E-, P- and A-sites. However, replacing of the original *gltX* Ser₁₀ codon AGC with 5 other synonymous codons had a negligible effect upon drug-induced stalling, whereas substituting it with an Ala codon significantly diminished translation arrest (Extended Data Fig. 6c). This result argues that it is the nature of the nascent peptide's C-terminal amino acid, rather than that of the P-site tRNA, that drive the context specificity of EVN action.

The results of these experiments clearly show that it is not only the identity of the A-site codon but, rather, the interplay between C-terminal residues of the nascent peptide and the incoming aa-tRNA that define the sites of EVN action in the cell.

Context specific action of EVN controls resistance genes

We wondered whether, like with some other ribosome-targeting antibiotics²⁵, nature has exploited the context specific action of EVN to direct ribosome stalling at specific sites within regulatory regions of resistance genes. One of the OSM resistance genes, *emtA*, originally identified on an *Enterococcus faecium* transposon²⁶, encodes an rRNA methyltransferase that introduces a modification into the 23S rRNA nucleotide G2470 (*E. coli* numbering) in the drug binding site which prevents binding of OSMs and renders cells resistant to these antibiotics²⁶. Neither the *emtA* distribution, nor the mechanism of its regulation have been previously reported. By inspecting sequenced bacterial genomes, we found that *emtA* homologs can be identified in diverse firmicute bacteria (Extended Data Figs. 7 and 8). Analysis of the 5' untranslated regions (UTRs) revealed the presence of a conserved ORF, which we designated as *emtAL* (Fig. 4a, Extended Data Fig. 8). Remarkably, the 10–15 amino acid-long peptides encoded in *emtAL* ORFs contain a strictly conserved VFL sequence, one of the top EVN sensitive tripeptides that emerged from our Ribo-seq experiments (Fig. 3a and Supplementary Dataset). Indeed, toeprinting analysis revealed a prominent EVN-dependent translation arrest at the Phe₆ codon within the VFL motif of the *E. faecium* *emtAL* ORF (Fig. 4b). Alanine scanning of the EmtAL peptide showed that Ala substitutions of any of the VFL residues alleviated drug-induced stalling (Fig. 4c), confirming the key role of the VFL sequence in EVN-dependent ribosome arrest.

Having established the *emtAL* ORF as a possible natural target for context-specific EVN action, we used it as a model to get mechanistic insights of how EVN inhibits protein synthesis. Binding of EVN in the tRNA accommodation corridor could potentially interfere either with the transfer of the nascent protein to the incoming aa-tRNA or with

translocation of the ribosome after transpeptidation. Either of these scenarios is compatible with ribosomes stalling at the Phe₆ codon within the *emtAL* VFL motif. To test whether EVN inhibits peptide bond formation, we analyzed the nature of peptidyl-tRNA in the ribosome stalled by EVN on the *emtAL* template: if the drug interferes with peptide bond formation, then a large fraction of the stalled ribosomes would carry the 6-amino acid long nascent peptide MMMAVF esterified to the P-site tRNA^{Phe} (Fig. 4d). We prepared a truncated *emtAL* mRNA template coding for the first 7 amino acids of the EmtAL peptide, MMMAVFL (Fig 4d, top). This template was translated in a cell-free system containing [¹⁴C]-Phe. Taking advantage of the different electrophoretic mobilities of MMMAVF-tRNA^{Phe} and MMMAVFL-tRNA^{Leu} (Fig. 4d, lanes 2 and 3) we observed that in the absence of the drug, ribosomes stalled at the truncated mRNA 3' end carried almost exclusively MMMAVFL-tRNA^{Leu}, but in the presence of EVN accumulation of MMMAVF-tRNA^{Phe} was observed (Fig. 4d, lane 5). This result shows that EVN interferes with the transfer of the peptidyl moiety from MMMAVF-tRNA^{Phe} to Leu-tRNA^{Leu}. Inhibition of transpeptidation was antibiotic concentration dependent, but even at the highest tested drug concentration (500 μM), inhibition remained incomplete (Extended Data Fig. 9a), in full agreement with the results of toeprinting experiments showing that EVN induces ribosome pausing rather than complete translation arrest at the VFL motif of *emtAL* (Fig. 4c).

To determine whether EVN stalls the ribosome at the Phe₆ codon of the *emtAL* ORF also in vivo, we assembled a reporter cassette, *emtAL-ermCL*, based on the well-characterized inducible macrolide resistance gene *ermC*^{25,27}. Arrested by EVN within the VFL-coding segment, the ribosome would be appropriately positioned for activating expression of the downstream red fluorescent protein (RFP) reporter gene (Fig. 5a). Drop-diffusion test revealed EVN mediated activation of RFP (Fig. 5b), reflecting drug-dependent ribosome stalling at the VFL sequence. Furthermore, consistent with the results of the in vitro alanine scanning (Fig. 4c), mutating the Leu residue of VFL to Ala significantly diminished the reporter induction (Fig. 5b), confirming that the intact VFL sequence encoded in *emtAL* is required for EVN-dependent programmed translation arrest in vivo. No reporter expression was observed upon treatment of cells with spectinomycin (SPC), an unrelated translation inhibitor (Fig. 5b). Inducible expression of the reporter at subinhibitory EVN concentrations was similarly observed in liquid culture experiments (Fig. 5c).

Taken together, our results strongly argue that programmed translation arrest at the VFL tripeptide encoded in the *emtAL* leader ORF is likely used for regulation of expression of the *emtA* resistance gene. Furthermore, the sequence of the EmtAL peptide has been likely evolutionarily selected to facilitate sensing the antibiotic presence by utilizing the nascent protein and acceptor amino acid requirements for the context-specific action of OSM antibiotics.

Discussion

Our data show that EVN and likely other antibiotics of the OSM class inhibit translation elongation by arresting ribosomes at particular mRNA sites encoding specific amino acid sequences.

Previous in vitro experiments had indicated that EVN may interfere with IF2 dependent formation of the 70S initiation complex^{5,8}. However, our in vivo (Ribo-seq and polysome profiling) and in vitro (toeprinting) experiments show that interference with translation initiation plays only a minor role in inhibition of cellular translation by EVN. We uncovered that instead, EVN preferentially arrests translation elongation when ribosomes try to polymerize certain tripeptide motifs. The nature of the incoming aa-tRNA and the properties of the nascent peptide apparently define the sites of EVN action. The codon bias at the A site of the EVN-stalled ribosome (Fig. 2a) reveals the importance of the codon-anticodon interactions. This conclusion is strongly supported by the observation that replacing the Arg codon CGU with CGA, which are decoded by the same tRNA_{2^{Arg}} (ICG), promotes drug-induced ribosome pausing (Fig. 2b). While inosine in the tRNA_{2^{Arg}} anticodon base pairs with U, C and A in the wobble position of CGN codons²⁸, decoding of CGA is less efficient²⁹. Weaker pairing of aa-tRNA with the A-site codon likely favors EVN-induced ribosome stalling. Conceptually similar is the situation with the Ile codon AUA which, unlike the other two Ile codons, is conducive to EVN-induced stalling (Fig. 2a). The lysinylation of the cytidine of the tRNA_{2^{Ile}} anticodon CAU^{30,31} allows its pairing with the adenine in the wobble position of the AUA codon, albeit forming a weaker interaction³², which presumably favors EVN action. We further noticed that the tRNAs decoding all the Pro (CCN) and Leu (CUN) codons and the Arg codon CGG, found at sites of preferred EVN action (asterisks in Fig. 2a), are exclusively modified by the TrmD methyltransferase at the G37 position immediately adjacent to the anticodons^{33,34}, presumably to alleviate the intrinsically problematic decoding of the codons starting with cytosine. However, the m¹G37-mediated compensation may be insufficient, making the accommodation of the corresponding aa-tRNAs particularly sensitive to EVN.

The presence of specific codons in the A site is important but insufficient for prominent EVN action (Extended Data Fig. 5b). Ribosomes are more prone to EVN-induced stalling when, in addition to having problematic codons in the A site, carry peptidyl-tRNAs esterified with distinct nascent polypeptides. Drug action is particularly influenced by the properties of the two C-terminal residues of the growing protein. Because EVN interferes with the transfer of the nascent peptide to the incoming aa-tRNA (Fig. 4d) and its action is affected by the features of the donor and acceptor substrates of transpeptidation, EVN specificity is likely determined by events occurring at the PTC.

The majority of EVN stalling tripeptide motifs resemble known poor substrates of transpeptidation. Most of the identified motifs contain one or several proline residues (Fig. 3b), which are known to slow down transpeptidation^{35–38} even when present in the penultimate position of the nascent polypeptide^{22,39}. (While synthesis of proline-rich motifs is facilitated by translation factor EF-P^{37,38}, the factor seems to be unable to relieve EVN-induced arrest: in our MIC tests, *efp* mutant of *Bacillus subtilis*⁴⁰ showed no increased sensitivity towards EVN). Another prominent EVN-stalling sequence, Arg/Lys-X-Arg/Lys (the “+X+” motif) (Fig. 3b), is known to be problematic for bacterial ribosomes²³ becoming particularly precarious when macrolide antibiotics bind in the exit tunnel^{16,17,24,41}. Translation of this motif by eukaryotic ribosomes requires the assistance of a specialized elongation factor⁴². Lastly, the EVN-susceptible P,X,[D/E] motif (Fig. 3b) resembles sequences whose translation promotes ribosome splitting possibly due in part

to inefficient peptide bond formation^{43,44}. Other EVN stalling motifs, which had not been previously implicated in translation problems, may become onerous only when the drug is present.

While our data argue that EVN action is controlled in part by the growing peptide, we cannot completely rule out that instead the E- and P-site tRNAs are the critical factors influencing the drug action. However, a strong argument favoring our peptide-centered view is that the efficiency of EVN-induced ribosome stalling is affected not only by the tripeptide sequence (and thus, possibly, ribosome-associated tRNAs) but also by more distal segments of the nascent protein, where ribosome-bound tRNAs are irrelevant. Thus, changing the EmtAL sequence preceding the VFL stalling motif from MMMAVFL to MNDGVFL significantly reduces EVN arrest (Extended Data Fig. 9b). The peptide-centric view is further supported by our observation that synonymous P-site Ser-codon replacement within the PSP stalling motif only weakly affect EVN-induced stalling whereas missense mutations had a pronounced effect (Extended Data Fig. 6b,c).

How OSMs, that bind in the tRNA accommodation corridor nearly 50 Å away from the PTC^{6,7} can affect transpeptidation? The possible explanation comes from the single-molecule studies showing that in the EVN-bound ribosome, aa-tRNA can briefly reach a near-accommodated state but then rapidly bounces back, and after several such futile attempts eventually dissociates from the ribosome¹². Therefore, OSMs likely affect peptide bond formation by either reducing the residence time of the aa-tRNA in the A site or preventing the proper placement of the acceptor amino acid in the PTC. Based on our findings, we propose that OSMs preferentially arrest translation when the combinations of the P- and A-site PTC substrates is unfavorable for rapid peptide bond formation in the drug-bound ribosome. Clash of the antibiotic with the elbow of the A-site aa-tRNA^{6,7} likely allows for a brief excursion of its aminoacylated acceptor end into the PTC (Fig. 6A, states I-II). Even such a transient visit may be sufficient for forming a peptide bond with most donor substrates, allowing transfer of the nascent chain to the incoming tRNA (Fig. 6A, state III). Anchored now in the ribosome by the nascent chain, the A/P-state peptidyl-tRNA could either expel the antibiotic (Fig. 6a, state IIIa), or allow translocation without displacing the inhibitor (Fig. 6a, state IV). When, however, the nascent protein ends with an unfavorable amino acid sequence, either the orientation or the dynamics of its C-terminal residue in the P site is inadequate for rapid transpeptidation during the fleeting visit of the acceptor substrate into the PTC (Fig. 6b, state V). As a result, the A-site bound aa-tRNA swings away from the PTC and, after several similarly unproductive attempts, is eventually rejected¹² (Fig. 6b, states VI and VII). Weak or inefficient codon-anticodon interactions would allow for fewer excursions of the acceptor end of aa-tRNA into the PTC prior to tRNA dissociation.

Our discovery of context specificity of action of OSM antibiotics illuminates the principle of antibiotic sensing required for inducible expression of resistance genes. The broad use of avilamycin used as a farm animal growth promoter, selected for *Enterococcal* strains that express the rRNA methyltransferase EmtA, which modifies 23S rRNA residue G2470 located in the tRNA accommodation corridor and confers OSM resistance^{26,45}. The *emtA* gene found in farm isolates likely originated in environmental bacterial strains (Extended Data Figs. 7 and 8) possibly encountering OSM antibiotics secreted by the microbial

producers in their natural habitats. Because rRNA modifications installed by resistance enzymes are often associated with a high fitness cost⁴⁶ the encoding genes are often expressed only when the antibiotic is present. In a common scenario, drug-dependent ribosome stalling at a defined site within the upstream ORF triggers mRNA re-folding alleviating transcriptional or translational attenuation of the resistance cistron²⁵. The presence of an upstream ORF *emtAL* encoding a short leader peptide with the conserved VFL sequence that directs EVN-dependent ribosome stalling (Fig. 4a), is a strong indication that expression of *emtA* genes is controlled by OSM-mediated programmed translation arrest. Potential base-pairing of the *emtAL*-coding sequence with the more distant 5'UTR segments (Extended Data Fig. 10) hints that ribosome stalling within the *emtAL* ORF could significantly remodel mRNA folding leading to gene activation. Thus, nature likely exploits context specificity of OSMs for antibiotic sensing and regulating expression of resistance genes.

The VFL sequence exploited for antibiotic sensing is not the strongest EVN arrest motif (Fig. 3c), as a sizeable fraction of translating ribosomes escape the EVN-dependent arrest (Fig. 4c,d). Nevertheless, the degree of EVN-induced ribosome stalling afforded by the VFL motif is likely optimal for achieving the adequate level of EmtA expression to confer antibiotic resistance without compromising too severely the activity of cellular ribosomes. Several EVN stalling motifs are present in the sequence of the EmtA gene itself; therefore, its translation is likely inhibited at high concentrations of the antibiotic. The EmtAL-EmtA system is presumably evolutionarily optimized for activation of resistance at subinhibitory concentrations of OSMs, when there are still enough drug-free ribosomes to allow production of the EmtA methylase.

In conclusion, our in vivo and in vitro studies revealed an unorthodox mode of action for an important class of ribosome targeting antibiotics. Our findings provide insights into the functions of the ribosome itself and illuminate principles of regulation of resistance mechanisms.

Methods

Toeprinting assays.

DNA templates for toeprinting were generated by PCR using AccuPrime DNA Polymerase (Thermo Fisher). The names and sequences of all the primers are listed in Supplementary Table. The *hupA*, *mgo* and *greA* templates were amplified from *E. coli* genomic DNA using primers T7-xxx-FWD and xxx-REV-NV1, where 'xxx' represents the name of the corresponding gene. The *hns* template was prepared using 4-primer PCR⁴⁸ using primers T7, NV1, hsn-FL_FWD, and hns-REV-trunc. The *ermBL*, *emtAL* and related mutant templates were synthesized via 5 primer PCR, using 4 common primers, T7 and NV1 at 100 μ M, T7-EmtAL-Fwd1 and NV1-EmtAL-Rev primers at 10 μ M, and an additional template-specific forward primer at 1 μ M. The *gltX* and related mutant templates were synthesized via 6 primer PCR, where T7 and NV1 were at 100 μ M, T7-gltX-fwd and gltX-rev-NV1 at 10 μ M, and gltX-2-fwd and gltX-rev at 1 μ M.

Toeprinting reactions were carried out in 5 μ L of PURExpress transcription-translation system (New England Biolabs) essentially as described in⁴⁹. EVN was added to the final concentration of 50 μ M unless otherwise stated. Where indicated, oncocin (Onc112) (GenScript) and retapamulin (RET) (Sigma-Aldrich) were added to a final concentration of 50 μ M. Following 10 min of translation, reverse transcription was carried out for 10 min using toeprinting primer NV1. Reverse transcription products were separated on a 6% sequencing gel. The gel was dried, exposed to a phosphorimager screen, and visualized in a Typhoon phosphorimager (GE Healthcare).

Polysome analysis.

E. coli imp4213 cells¹⁹ were grown in 40 mL of LB media to a density of $A_{600} \sim 0.5$, split into separate flasks and either treated with 100x MIC of EVN for 4 min, 1x MIC of EVN for 30 minutes, or left untreated (control). Cells were pelleted in a JA-25.50 (Beckman) rotor pre-warmed to 37 °C at 8000 rpm (7720 \times g) for 3 min, resuspended in 650 μ L cold lysis buffer (20 mM Tris, pH 8.0, 10 mM $MgCl_2$, 100 mM NH_4Cl , 5 mM $CaCl_2$, 0.4 % Triton-X100, 0.1% NP-40) supplemented with 65 U RNase-free DNase I (Roche), 208 U Superase•In™ RNase inhibitor (Invitrogen) and 1 mg/ml chloramphenicol and snap frozen in liquid nitrogen and cryo-lysed. Lysates were centrifuged at 20,000 \times g for 30 min at 4 °C and polysomes-containing supernatant was loaded onto a 10–50% sucrose gradient (prepared in a buffer containing 20 mM Tris-HCl, pH 8.0, 10 mM $MgCl_2$, 100 mM NH_4Cl). Ribosomes and polysomes were resolved by centrifugation in a SW-41 rotor at 39,000 rpm (260000 \times g) for 2 h at 4 °C. Gradients were fractionated using a Gradient fractionator (BioComp) with UV detection at 254 nm.

Protein synthesis inhibition assay.

Inhibition of cellular protein synthesis by EVN was analyzed by metabolic labeling²⁰ with the following modifications. *E. coli* imp4213 cells¹⁹ were grown overnight in LB medium. Cells were diluted 1:200 into MOPS media lacking methionine (Teknova) (MOPS Met) and grown at 37°C until the culture reached a density of A_{660} of 0.2. EVN diluted in MOPS Met media was added to the exponentially growing cells to obtain a final antibiotic concentration of 50 μ M. At 0.5, 1, 2, 4, 8 and 16 min, aliquots of 28 μ L were transferred to another tube containing 2 μ L MOPS Met medium supplemented with 0.3 μ Ci of L-[³⁵S]-methionine (specific activity 1,175 Ci/mmol) (MP Biomedicals). Following 90 s incubation, the content was transferred onto Whatman 3MM paper discs pre-wetted with 5% TCA. The discs were placed in a beaker with 500 mL 5% TCA and boiled for 5 min. TCA was discarded and the washing step was repeated one more time. After rinsing the discs in acetone they were air-dried and placed in scintillation vials. After addition of 5 mL of scintillation cocktail the amount of retained radioactivity was measured in a scintillation counter. For the control sample without antibiotic, an aliquot of the cell culture immediately before dosing with EVN was taken and transferred to medium with L-[³⁵S]-methionine as described for the time course samples.

Cell growth and cell lysates preparation for Ribo-seq experiments.

The Ribo-seq experiments were performed as described previously²⁰ using cells grown in LB medium. Briefly, the overnight cultures of *E. coli* imp4213 cells were diluted 1:200 in

150 mL of LB medium and grown at 37°C in flasks until reaching density of $A_{600} \sim 0.4$. For EVN-treated samples, EVN was added to the cultures to a final concentration of 50 $\mu\text{g}/\text{mL}$ (100X MIC) from a stock solution in 100% ethanol, and incubation with shaking continued for 4 min. Untreated (control) and EVN-treated cells were harvested by rapid filtration, flash frozen in liquid nitrogen and cryo-lysed in 650 μL lysis buffer (20 mM Tris, pH 8.0, 10 mM MgCl_2 , 100 mM NH_4Cl , 5 mM CaCl_2 , 0.4 % Triton-X100, and 0.1% NP-40) supplemented with 65 U RNase-free DNase I (Roche) and 208 U Superase•In™ RNase inhibitor (Invitrogen). The pulverized cells were thawed at 30°C for 2 min, incubated in an ice water bath for 20 min, and lysates were clarified by centrifugation at $20,000 \times g$ for 10 min at 4°C. Clarified lysates were immediately treated with 450 U MNase (Roche) per 25 A_{260} units of lysate and 3 mM GMPPNP and were incubated for 60 min at 25°C. The MNase reaction was quenched by addition of 5 mM EGTA (final concentration). Following sucrose gradient centrifugation and collection of the 70S ribosome peak⁵⁰, subsequent isolation of ribosomal footprints and library preparation were performed as described in two different protocols^{15 51}, one for each set of biological replicates.

Processing of ribosome footprints for Ribo-seq analysis.

For the biological replicate prepared by the protocol of⁵¹ library preparation protocol, a custom script was used to demultiplex the samples, remove the linker barcode and any nts 3' of the linker barcode, and then remove 5 nts from the 3' end and 2 nts from the 5' end, which were added as part of the library design^{51,52}. For the biological replicates following the library preparation protocol described in¹⁵, samples were not multiplexed, but the same custom script was used to identify and remove the 3' adapter sequence and then remove 1 nt from the 5' end. The remainder of the data processing between biological replicates was the same. Bowtie2 (v2.2.9) within the GALAXY pipeline first aligned the trimmed reads to the non-coding RNA sequences. The remaining unmapped reads were aligned to the reference genome of the *E. coli* strain MG1655 (GenBank ID [U00096.3](#)), which is the parent of the strain imp4213 used in Ribo-seq experiment. The 23 to 40 nt-long reads were used in the subsequent analyses. After analyzing the footprints at the start codons, the first position of the P-site codon was assigned 15 nt from the 3' end of the read.

Metagene analysis.

The metagene analyses at the annotated start and stop regions followed the described protocol⁵³. Included in the analysis were the ORFs that were: a) separated by at least 50 nt; b) with the length of 300 nt or more; c) with at least 20% of the positions had assigned reads values above zero; d) with the average number of RPM per nt > 0.005 . For the metagene plots, ribosome footprint density was normalized to the average coverage of the ORF including 50 flanking nts. The mean of the normalized values was computed and plotted for the ORF segments around the start and stop codons.

The metagene analysis at specific tripeptide sequences was carried out by first identifying such motifs in the bodies of the genes, ignoring those in the first and last 30 nts of the ORFs. Normalized read coverage, calculated for each nucleotide within a 200 nt window centered around the middle nucleotide of the P-site, was determined by dividing ribosome footprint

coverage at each position by the maximum coverage value within the window. Normalized coverage was then summed for each position in the windows and plotted.

Calculation of EVN stall scores.

The *EVN stall score* is calculated on a codon-by-codon basis throughout the genome according to the formula:

$$EVN\ stall\ score = \log_2\left(\frac{normalized\ codon\ RPM\ Evn\ sample}{normalized\ codon\ RPM\ control\ sample}\right)$$

P-site assigned reads (15nt offset from 3' end of read) are used in all the analyses. Each codon RPM value is normalized to the total gene RPM. For a codon to be included in the analysis, in both the control and the EVN samples it needs a minimum of 5 aligned reads and for the gene to have a minimum of 100 aligned reads.

For the analysis of the A-site codon EVN stall score, the *A-site codon stall score* is defined as the *average EVN stall score* (above formula) when each of the 61 sense codons in the A-site. Codons needed to pass the minimum codon and gene read thresholds as described above, and codons 2 and 3 of each gene were excluded from analysis to mitigate any effects of initiation or context of fMet in the P or E sites.

Similarly, for the tripeptide EVN stall score analysis, the *EVN tripeptide stall score* is defined as the *average EVN stall score* when each tripeptide sequence is centered on the P site. Codon 2 of each gene was excluded such that fMetXX motifs were not considered in the calculations. Furthermore, tripeptides with fewer than 10 occurrences were omitted from plots and further consideration.

EmtA alignment and identification of putative small ORFs.

The most closely related protein sequences to EmtA were retrieved from NCBI (<https://www.ncbi.nlm.nih.gov/>) via a BlastP search against the “nr” database with E value limit 1e-100. A representative set of more distant relatives was retrieved via a BlastP search against a limited set of genomes (one per species) available through the webFlaGs server with E value limit 1e-10⁵⁴. The two sequence sets were merged, aligned with MAFFT L-ins-I (v.7)⁵⁵, and cut down to the most closely aligning sequences (54 unique protein sequences). After removing alignment positions with more than 50% gaps with TrimAL v1.4.rev6⁵⁶, phylogenetic analysis was carried out with IQTree version 2.1.2 on the CIPRES server with 1000 rapid bootstrap replicates and automatic model detection^{57,58}.

The upstream 700 nucleotide positions for the genes coding for the 54 EmtA homologues was extracted using the eUIGene.py Python script (<https://github.com/GCA-VH-lab/eUIGene>), using the results of a FlaGs search with the -r 10 option as input⁵⁴. These 5'UTR regions were aligned with MAFFT L-ins-i and visualized with Aliview⁵⁹. Conserved regions were identified by eye, enabling the detection of a Shine-Dalgarno-like region, followed by a short ORF-like region in multiple genomes. This ORF was translated to putative peptide sequences with Aliview.

Rho-independent transcription terminator sequences were predicted with the Arnold server (<http://rssf.i2bc.paris-saclay.fr/toolbox/arnold/>).

Testing inducible gene expression by EVN-mediated programmed translation arrest.

An EVN-responsive reporter plasmid was constructed based on the inducible *ermCL-RFP* plasmid, where expression of RFP originally depends on macrolide-mediated stalling on the leader *ermCL* region. The first 10 codons of *ermCL* of the reporter's *ermCL-RFP* sequence were replaced with the first 7 codons of *emtAL*, which include the VFL₇ EVN stalling sequence, to obtain the chimeric wt-*emtAL(VFL)*-*ermCL-RFP* reporter plasmid. In addition, by changing the Leu7(UUG) codon of *emtAL* to code for Ala (GCG), we also generated the mutant *emtAL(VFA)*-*ermCL-RFP* reporter plasmid. Both wt and mutant plasmids were introduced into *E. coli* BW25113 cells which are rendered EVN sensitive by expressing the Pore protein from an arabinose-inducible chromosomal cassette⁶⁰. A lawn of cells from overnight cultures were plated on LB-agar media containing 100 µg/mL Amp, 50 µg/mL Kan, 0.2 mM IPTG and 0.1% L-arabinose. A 1 µL drop each of EVN in DMSO at 20 mg/mL and spectinomycin in water at 10 mg/mL were spotted onto the lawn of cells. After 18 h at 37°C, the plates were imaged on ChemiDoc MP (Biorad).

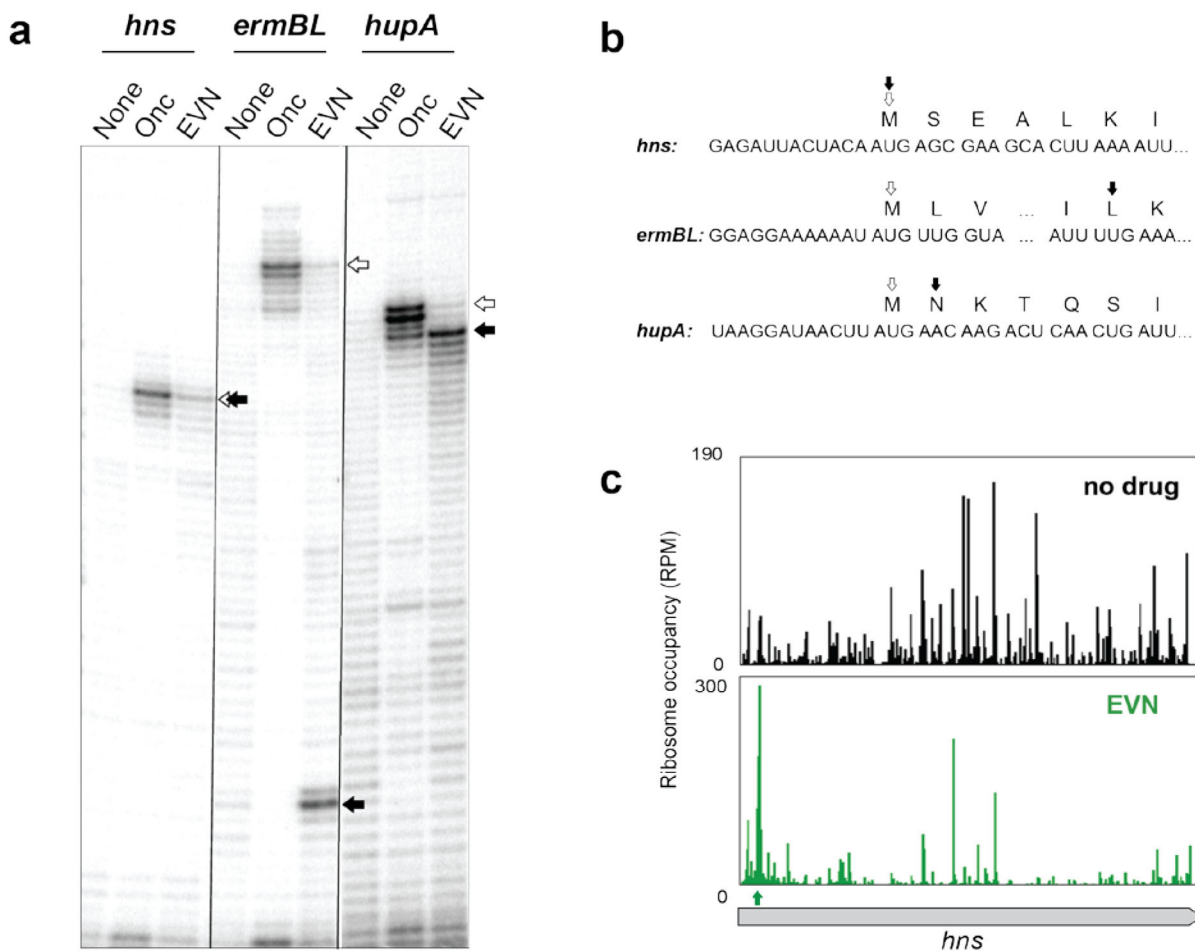
For the liquid culture experiments (Fig. 5c), the same strains that were used for the drop-diffusion experiments were grown overnight in LB medium supplemented with 100 µg/mL Amp and 50 µg/mL Kan. Cells were then diluted 1:100 in LB medium supplemented with the same antibiotics and grown to OD₆₀₀ ~ 0.5–0.8. Cells were further diluted in LB medium containing Amp (100 µg/mL), Kan (50 µg/mL), IPTG (0.2 mM) and arabinose (0.1%) and placed in the wells of the 96-well black-wall/clear-bottom plate. The wells were then supplemented with the same medium containing varying concentrations of either EVN or spectinomycin. The final culture volume in wells was 180 µL. Drug concentrations varied from 0 to 0.5 µg/mL over 1.25-fold dilutions. Cells were grown in the TECAN plate reader at 37°C with monitoring every 20 min of cell density (OD₆₀₀) and RFP fluorescence ($\lambda_{\text{ex}} = 550 \text{ nm}$, $\lambda_{\text{em}} = 675 \text{ nm}$, gain 30%).

In vitro translation of *emtAL* templates.

Templates devoid of a stop codon encoding EmtAL peptides MMMAVF and MMMAVFL were generated by PCR similar to that used to generate the *emtAL* template but using unique reverse primers (Supplementary Table).

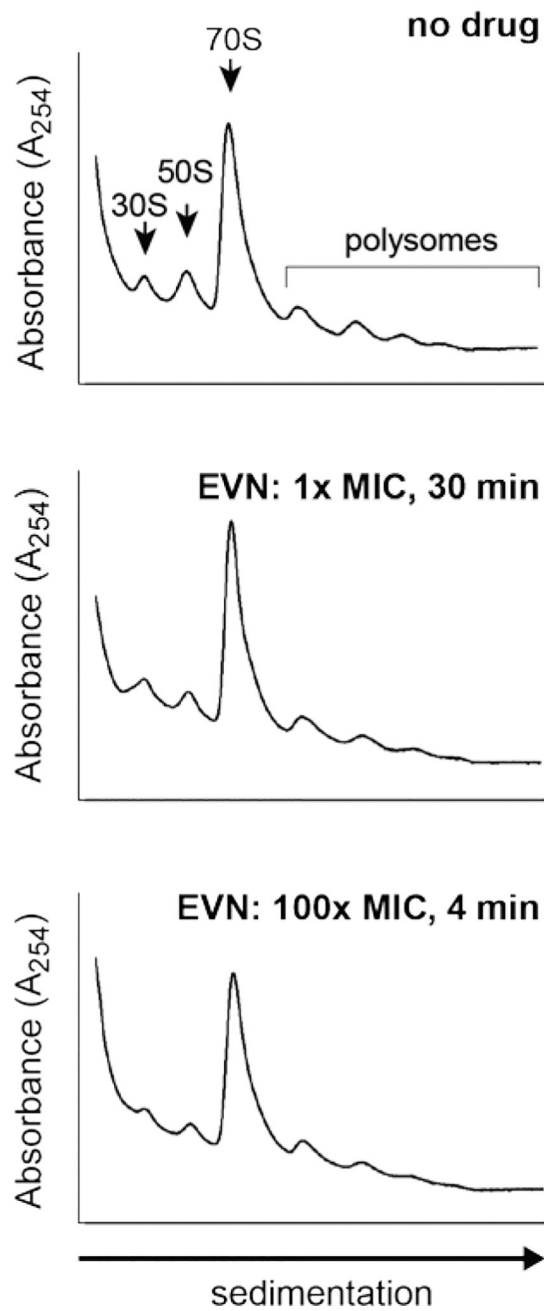
In vitro translation reactions were carried out in 5 µL of PURExpress transcription-translation system (New England Biolabs) supplemented with 0.09 µCi of [¹⁴C]-Phe (487 mCi/mmol specific activity) (Perkin Elmer). Where indicated, EVN was added to a final concentration of 500 µM. Following translation for 30 min at 37°C, a × µL aliquot of the reactions were treated with 0.5 µg of RNase A. Translation products were analyzed in a 16.5% Bis-Tris gel. Gels were dried and visualized in a Typhoon phosphorimager (GE Healthcare).

Extended Data



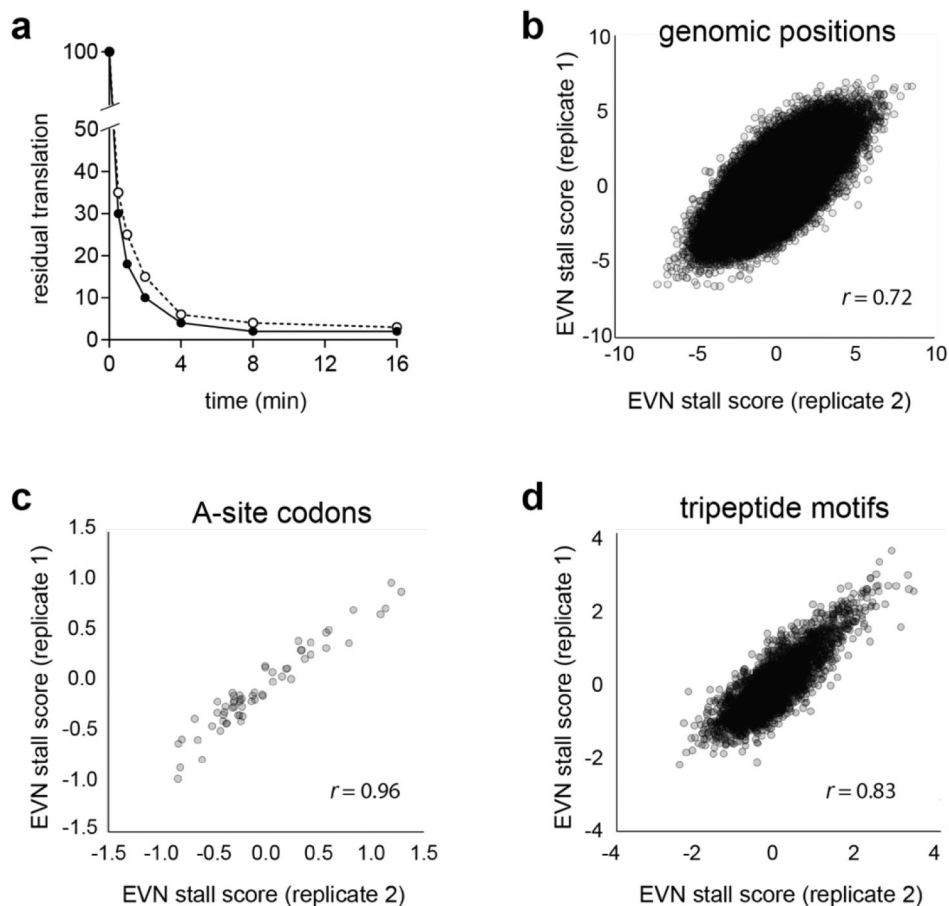
Extended Data Fig. 1. Action of EVN is gene specific and does not involve an obligatory translation initiation arrest.

a, In vitro toeprinting experiments to analyze EVN-dependent translation arrest. Selection of the model genes was based on the results of Ribo-seq analysis (*hupA*) or those tested in previous reports (*hns* and *ermBL*)^{7,13}. Open arrows indicate toeprint bands representing ribosomes stalled at the start codons by the action of initiation inhibitor oncocin (Onc)²¹. Black arrows point to the bands representing EVN-stalled ribosomes. Shown is a representative gel from at least two independent experiments. **b**, The nucleotide sequences of the relevant portions of the mRNA templates used in the toeprinting experiments shown in (a) and amino acid sequences of the encoded proteins. The open and filled arrows are as in (a). **c**, Ribosome profiling does not show any pronounced EVN-induced ribosome stalling at the *hns* start codon in *E. coli* cells. The first strong drug-induced translation arrest (green arrow) occurs at the codon 5 of *hns*.



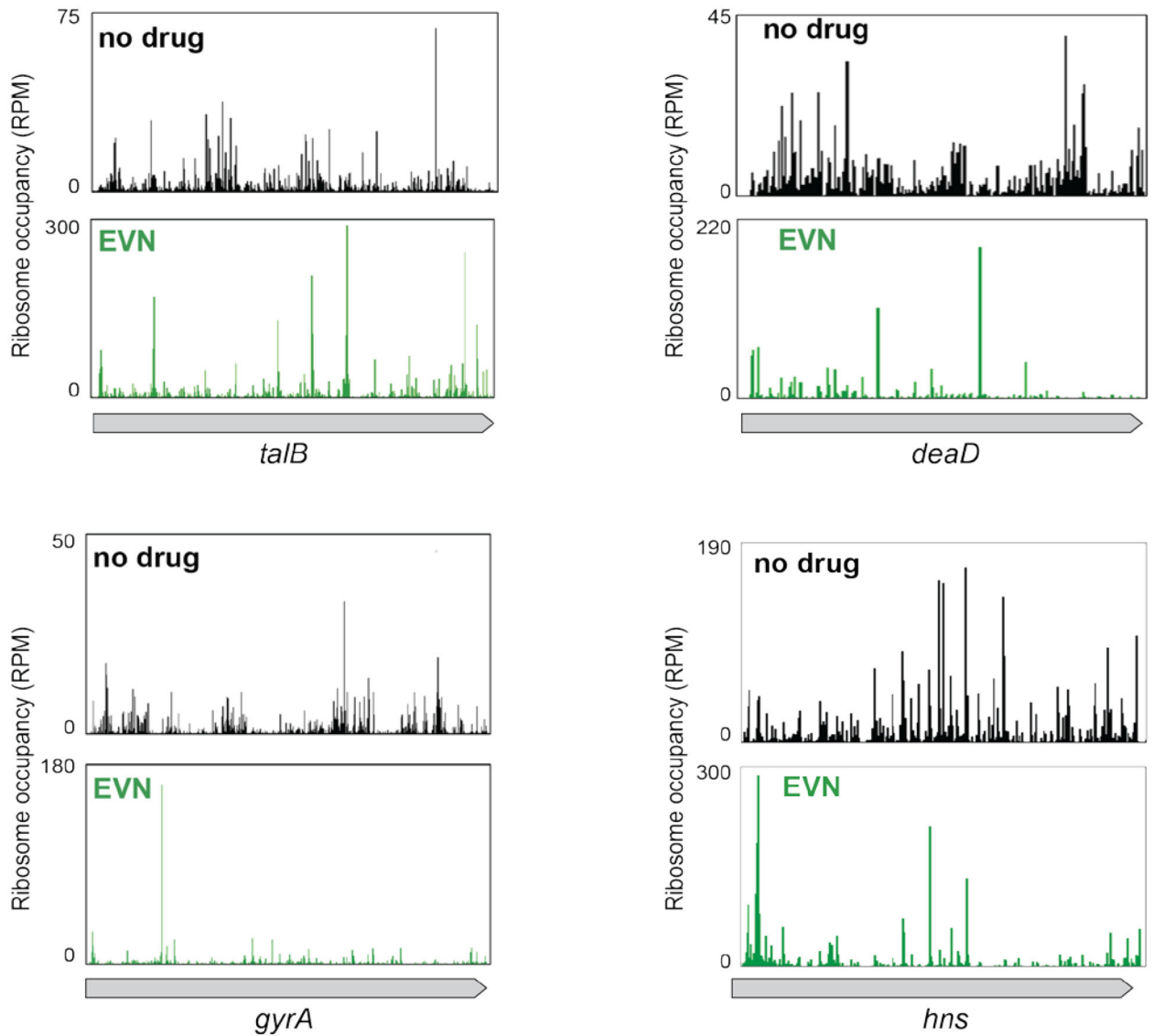
Extended Data Fig. 2: EVN preserves the polysome profiles.

Sucrose gradient analysis of polysomes prepared from untreated *E. coli* cells (no drug) or treated with 0.5 $\mu\text{g}/\text{mL}$ (1x MIC) or with 50 $\mu\text{g}/\text{mL}$ (100x MIC) EVN during 30 min or 4 min, respectively.



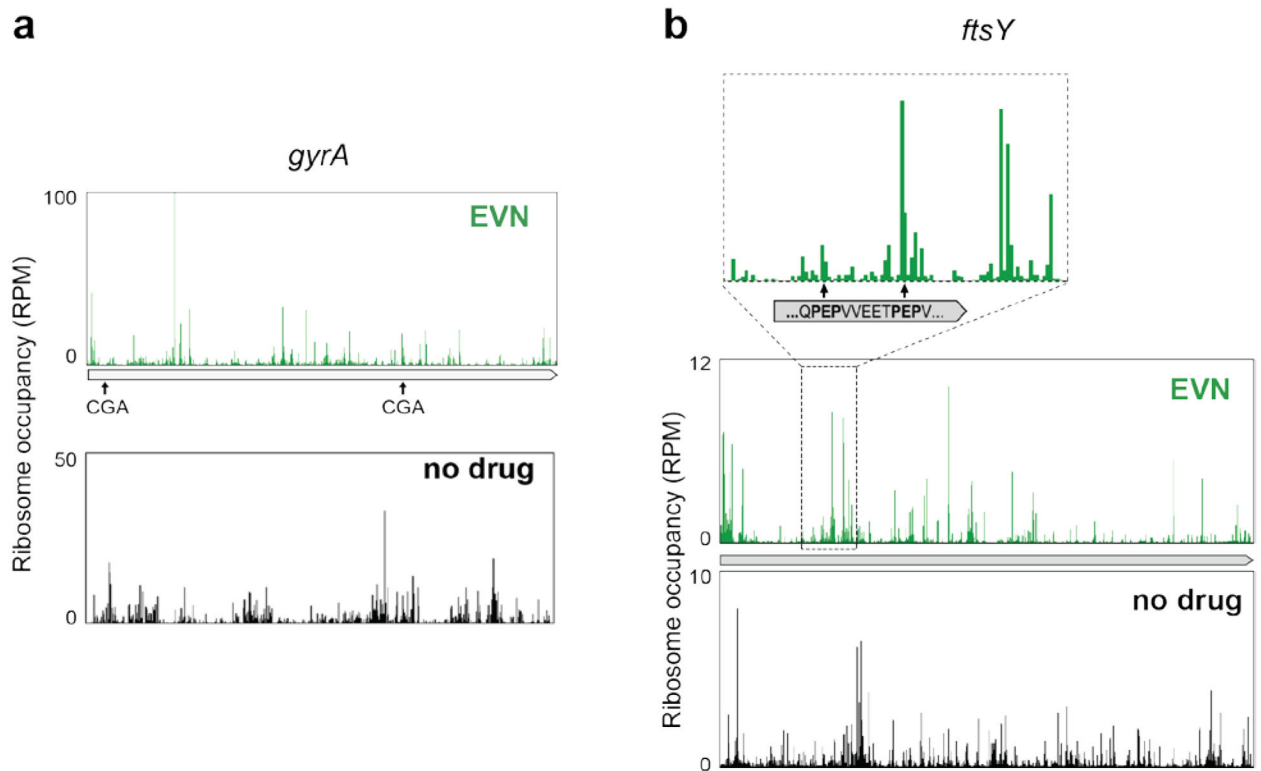
Extended Data Fig. 3: Conditions and reproducibility of the Ribo-seq experiments to elucidate the mode of action of EVN.

a, Residual global protein synthesis (evaluated as incorporation of [³⁵S]-Met into the TCA-insoluble protein fraction) of *E. coli* cells exposed to 50 μg/mL EVN for 4 min. Incorporation of [³⁵S]-Met in a sample of the bacterial culture taken right before the addition of EVN was set as 100%. Open and closed circles represent the results of two independent experiments. **b-d**, Reproducibility of the two independent Ribo-seq experiments as judged by: **(b)** the EVN stall scores of all the considered codon positions ($n = 118,222$, Pearson's $r = 0.72$); **(c)** of the mean stall score for codons at the ribosomal A site ($n = 61$, Pearson's $r = 0.96$); **(d)** of the mean score for considered tripeptide motifs ($n = 4039$, Pearson's $r = 0.83$) described in Figs. 2 and 3.



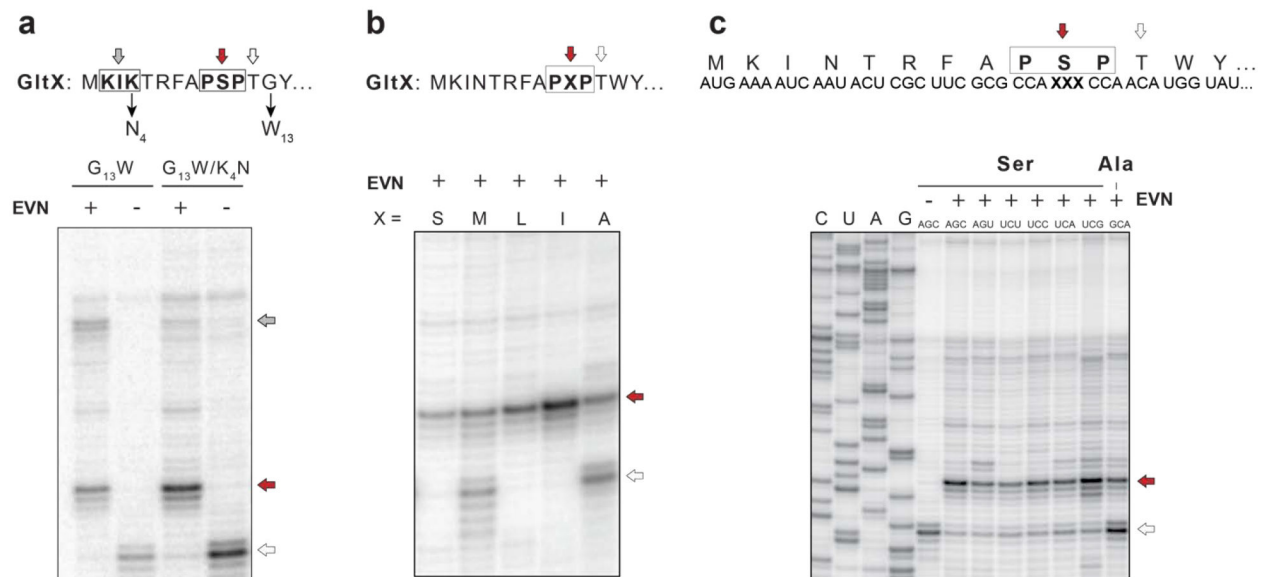
Extended Data Fig. 4: The action of EVN in bacterial cells is context specific.

Comparison of ribosome occupancy profiles of individual genes in untreated cells (no drug) with those treated with EVN.



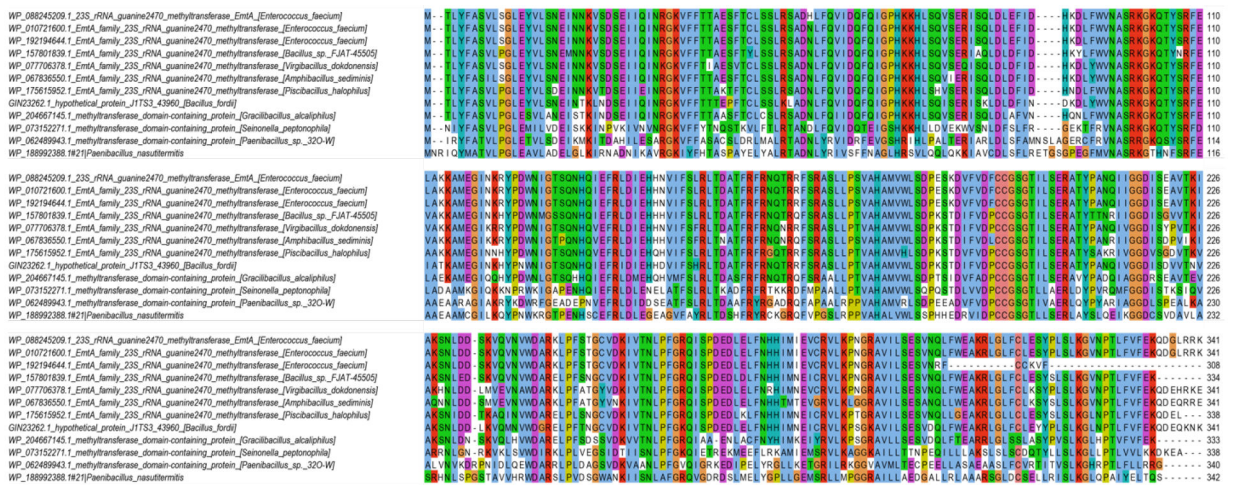
Extended Data Fig. 5: An extended sequence motif is required for EVN-dependent ribosome stalling.

a,b, Ribosome occupancy profiles of individual genes where, in the presence of EVN, ribosomes translate successfully or not CGA codons (**a**) or PEP sequences (belonging to the identified PXP EVN-arrest motif, see Fig. 3a, b) (**b**).



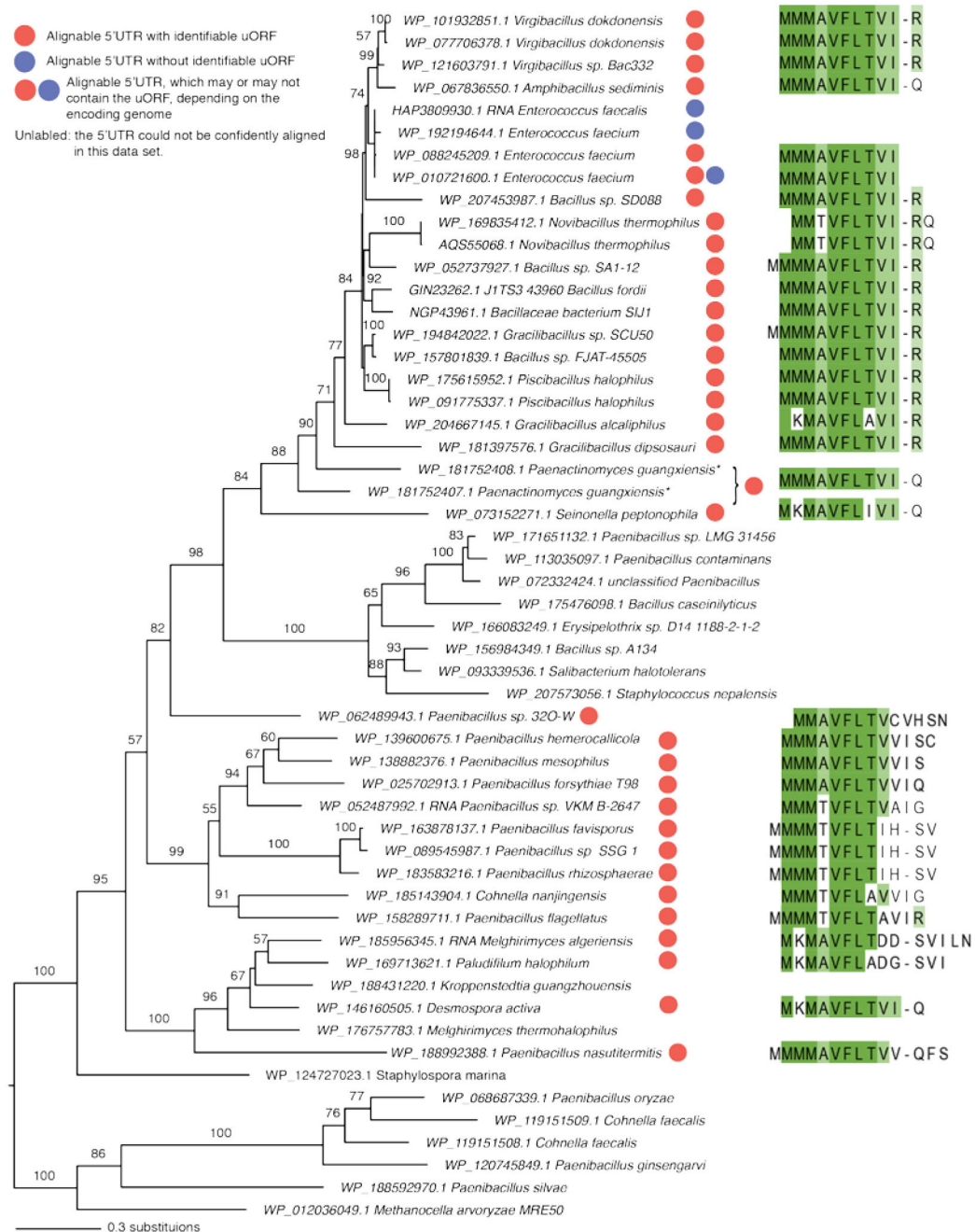
Extended Data Fig. 6: EVN-mediated ribosome stalling at a tripeptide PSP exemplifying the PXP motif.

a, Modifications of the *gltX* template to facilitate toeprinting analysis of EVN-mediated stalling at the PSP arrest sequence. The thin arrows indicate the mutations introduced in the wild-type sequence of the first 14 codons of the *gltX* gene encoding the EVN arrest motif Pro₉-Ser₁₀-Pro₁₁. Gly₁₃ codon was mutagenized to Trp₁₃ in order to trap translating ribosomes at the preceding Thr₁₂ (open arrow) when Trp-tRNA is depleted by the addition of indolmycin, an inhibitor of tryptophanyl-tRNA synthetase. In addition, the Lys₄ codon was mutagenized to Asn₄ codon to disrupt the +X+ motif Lys₂-Ile₃-Lys₄ of GltX, where mild EVN-mediated stalling occurs during in vitro translation (grey arrow). The red and open arrows indicate toeprint band representing EVN-bound ribosomes stalled at Ser₁₀ codon and the ribosomes trapped at the Thr₁₂ codon due to the depletion of Trp-tRNA, respectively. **b**, Toeprinting analysis of EVN-mediated ribosome stalling at the original PXP motif Pro₉-Ser₁₀-Pro₁₁ (X=Ser) of *gltX* or mutant templates where the Ser₁₀ codon was mutated to encode different amino acids (Met, Leu, Ile, or Ala). **c**, Synonymous mutations of the P-site Ser₁₀ codon have little effect of stalling, whereas replacement of the Ser₁₀ codon with the Ala codon has a strong effect. Representative gels from two independent experiments are shown in panels **a**, **b** and **c**.



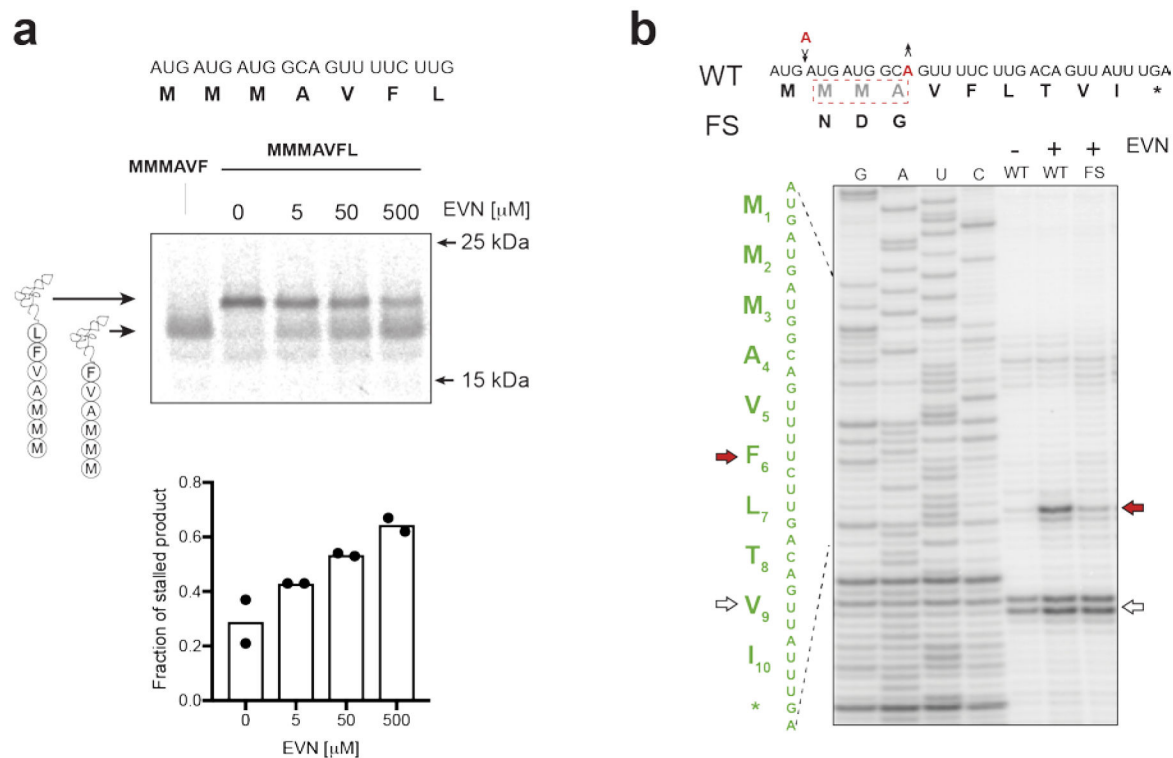
Extended Data Fig. 7. EmtA homologs are found in diverse bacterial species.

Alignment of representative EmtA sequences identified in sequenced bacterial genomes (see Extended Data Fig. 8 for the complete phylogenetic tree).



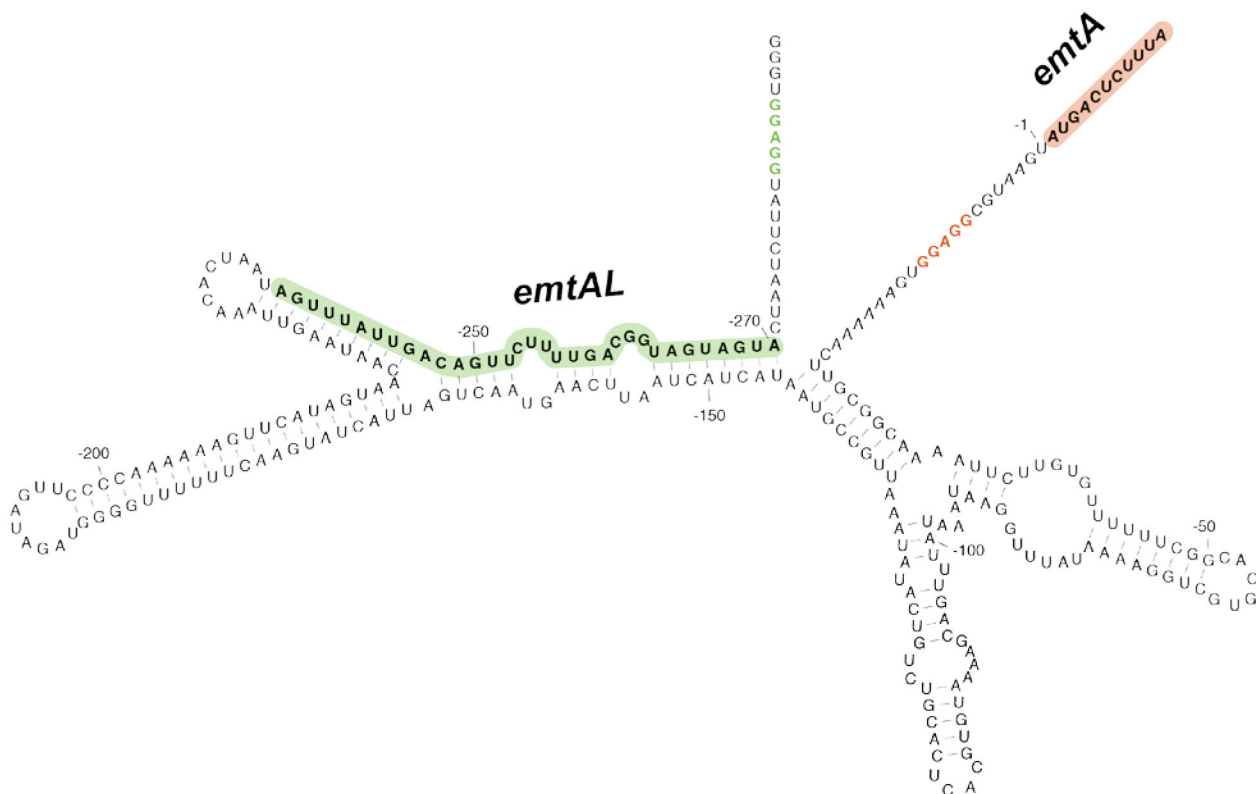
Extended Data Fig. 8. Maximum likelihood phylogeny of *emtA* homologs.

Branch lengths are proportional to the number of substitutions. The tree is annotated with circles showing the presence (red) or absence (blue) of the *emtAL* uORF in 5'UTR of the *emtA* genes, where the 5'UTR is confidently alignable. The sequences of the encoded leader peptides are indicated. The asterisk indicates peptides from two annotated neighboring ORFs in *Paenactinomyces guangxiensis*, corresponding to the N and C terminal regions of EmtA. The interruption of the *emtA* ORF suggests pseudogenation caused by a frameshift.



Extended Data Fig. 9. Distal segments of the nascent peptide in the ribosomal exit tunnel contribute to EVN-dependent translation arrest within the *emtAL* ORF.

a, The VFL motif within the *EmtAL* peptide affords only partial translation arrest. Top: gel electrophoretic analysis of accumulation of MMMAVF-tRNA and MMMAVFL-tRNA during in vitro translation of the truncated *emtAL* template at increasing concentrations of EVN. Bottom: quantification of the gel (two independent experiments) showing the fraction of incomplete translation product (MMMAVF-tRNA). **b**, Toeprinting analysis of EVN-mediated ribosome stalling in templates encoding the *E. faecium emtAL* ORF where the identities of codons 2–4 were simultaneously modified by introducing single-nucleotide compensatory frame-shifting mutations (indicated by black arrows and red letters). Representative gels from two independent experiments are shown in panels **a** and **b**.



Extended Data Fig.10. Leader ORF *emtAL* in the 5' UTR of the *E. faecium emtA* gene
Possible secondary structure of the 5'UTR of the *E. faecium emtA* gene. The *emtAL* ORF and its Shine-Dalgarno sequence are highlighted in green. The *emtA* ORF and its Shine-Dalgarno sequence are shown in red.

Supplementary Material

Refer to Web version on PubMed Central for supplementary material.

Acknowledgements

We thank Axel Innis and Elodie Leroy (University of Bordeaux) for structural insights, Sezen Meydan (University of Illinois at Chicago) for advice with some experiments, Maxim Svetlov for help with the figures and Michael Ibba (Ohio State University) for sharing the *B. subtilis* strains. We are grateful to Ya-Ming Hou (Thomas Jefferson University) for insights into the role of tRNA modification in decoding and to Paul Mann and Todd Black (Merck) for the advice on antibiotic-sensitive bacterial strains and information about preclinical development of evernimicin (Ziracin). This work was supported by the NIH grant R35-GM127134 to A.S.M.. K.M. was supported by a NIH Training Grant (5T32AT007533). G.C.A. was supported by grants from the Knut and Alice Wallenberg Foundation (KAW 2020.0037), Umeå University Medical Faculty (Biotechnology grant to G.C.A), Kempestiftelserna (SMK-1858.3 to G.C.A), Carl Tryggers Stiftelse för Vetenskaplig Forskning (CTS19:24), and the Swedish Research Council (2019-01085). C.K.S acknowledges support from Stiftelsen J.C. Kempes Stipendiefond.

Data availability

Ribosome profiling (Ribo-seq) data have been deposited to the Gene Expression Omnibus (GEO) database under accession number GSE193270.

References

1. McCranie EK & Bachmann BO Bioactive oligosaccharide natural products. *Natural product reports* 31, 1026–1042 (2014). [PubMed: 24883430]
2. McNicholas PM et al. Evernimicin binds exclusively to the 50S ribosomal subunit and inhibits translation in cell-free systems derived from both Gram-positive and Gram-negative bacteria. *Antimicrob. Agents Chemother* 44, 1121–1126 (2000). [PubMed: 10770739]
3. Lin J, Zhou D, Steitz TA, Polikanov YS & Gagnon MG Ribosome-targeting antibiotics: modes of action, mechanisms of resistance, and implications for drug design. *Annu. Rev. Biochem* 87, 451–478 (2018). [PubMed: 29570352]
4. Adrian PV et al. Evernimicin (SCH27899) inhibits a novel ribosome target site: analysis of 23S ribosomal DNA mutants. *Antimicrob. Agents Chemother* 44, 3101–3106 (2000). [PubMed: 11036030]
5. Belova L, Tenson T, Xiong L, McNicholas PM & Mankin AS A novel site of antibiotic action in the ribosome: interaction of evernimicin with the large ribosomal subunit. *Proc. Natl. Acad. Sci. USA* 98, 3726–3731 (2001). [PubMed: 11259679]
6. Krupkin M et al. Avilamycin and evernimicin induce structural changes in rProteins uL16 and CTC that enhance the inhibition of A-site tRNA binding. *Proc. Natl. Acad. Sci. USA* 113, E6796–E6805, (2016). [PubMed: 27791159]
7. Arenz S et al. Structures of the orthosomycin antibiotics avilamycin and evernimicin in complex with the bacterial 70S ribosome. *Proc. Natl. Acad. Sci. USA* 113, 7527–7532 (2016). [PubMed: 27330110]
8. Mikolajka A et al. Differential effects of thiopeptide and orthosomycin antibiotics on translational GTPases. *Chem. Biol* 18, 589–600 (2011). [PubMed: 21609840]
9. Wolf H Avilamycin, an inhibitor of the 30 S ribosomal subunits function. *FEBS lett* 36, 181–186 (1973). [PubMed: 4585189]
10. Gibbs MR et al. Conserved GTPase LepA (Elongation Factor 4) functions in biogenesis of the 30S subunit of the 70S ribosome. *Proc. Natl. Acad. Sci. USA* 114, 980–985 (2017). [PubMed: 28096346]
11. Choi E & Hwang J The GTPase BipA expressed at low temperature in *Escherichia coli* assists ribosome assembly and has chaperone-like activity. *J. Biol. Chem* 293, 18404–18419 (2018). [PubMed: 30305394]
12. Morse JC et al. Elongation factor-Tu can repetitively engage aminoacyl-tRNA within the ribosome during the proofreading stage of tRNA selection. *Proc. Natl. Acad. Sci. USA* 117, 3610–3620 (2020). [PubMed: 32024753]
13. Orelle C et al. Tools for characterizing bacterial protein synthesis inhibitors. *Antimicrob. Agents Chemother* 57, 5994–6004 (2013). [PubMed: 24041905]
14. Ingolia NT, Ghaemmaghami S, Newman JR & Weissman JS Genome-wide analysis in vivo of translation with nucleotide resolution using ribosome profiling. *Science* 324, 218–223 (2009). [PubMed: 19213877]
15. Oh E et al. Selective ribosome profiling reveals the cotranslational chaperone action of trigger factor in vivo. *Cell* 147, 1295–1308 (2011). [PubMed: 22153074]
16. Davis AR, Gohara DW & Yap MN Sequence selectivity of macrolide-induced translational attenuation. *Proc. Natl. Acad. Sci. USA* 111, 15379–15384 (2014). [PubMed: 25313041]
17. Kannan K et al. The general mode of translation inhibition by macrolide antibiotics. *Proc. Natl. Acad. Sci. USA* 111, 15958–15963 (2014). [PubMed: 25349425]
18. Vazquez-Laslop N & Mankin AS Context-specific action of ribosomal antibiotics. *Annu. Rev. Microbiol* 72, 185–207 (2018). [PubMed: 29906204]
19. Eggert US et al. Genetic basis for activity differences between vancomycin and glycolipid derivatives of vancomycin. *Science* 294, 361–364 (2001). [PubMed: 11520949]
20. Meydan S et al. Retapamulin-assisted ribosome profiling reveals the alternative bacterial proteome. *Mol. Cell* 74, 481–493 (2019). [PubMed: 30904393]

21. Weaver J, Mohammad F, Buskirk AR & Storz G Identifying small proteins by ribosome profiling with stalled initiation complexes. *mBio* 10, 02819–18 (2019).
22. Schuller AP, Wu CC, Dever TE, Buskirk AR & Green R eIF5A functions globally in translation elongation and termination. *Mol. Cell* 66, 194–205 (2017). [PubMed: 28392174]
23. Sothiselvam S et al. Binding of macrolide antibiotics leads to ribosomal selection against specific substrates based on their charge and size. *Cell Rep* 16, 1789–1799 (2016). [PubMed: 27498876]
24. Svetlov MS et al. Context-specific action of macrolide antibiotics on the eukaryotic ribosome. *Nat. Commun* 12, 2803 (2021). [PubMed: 33990576]
25. Weisblum B Insights into erythromycin action from studies of its activity as inducer of resistance. *Antimicrob Agents Chemother* 39, 797–805 (1995). [PubMed: 7785974]
26. Mann PA et al. EmtA, a rRNA methyltransferase conferring high-level evernimicin resistance. *Mol. Microbiol* 41, 1349–1356 (2001). [PubMed: 11580839]
27. Bailey M, Chettiath T & Mankin AS Induction of *ermC* expression by ‘non-inducing’ antibiotics. *Antimicrob. Agents Chemother* 52, 866–874 (2008). [PubMed: 18086834]
28. Cantara WA et al. Modifications modulate anticodon loop dynamics and codon recognition of *E. coli* tRNA(Arg1,2). *J. Mol. Biol* 416, 579–597 (2012). [PubMed: 22240457]
29. Curran JF Decoding with the A:I wobble pair is inefficient. *Nucleic Acids Res* 23, 683–688 (1995). [PubMed: 7534909]
30. Muramatsu T et al. Codon and amino-acid specificities of a transfer RNA are both converted by a single post-transcriptional modification. *Nature* 336, 179–181 (1988). [PubMed: 3054566]
31. Soma A et al. An RNA-modifying enzyme that governs both the codon and amino acid specificities of isoleucine tRNA. *Mol. Cell* 12, 689–698 (2003). [PubMed: 14527414]
32. Voorhees RM et al. The structural basis for specific decoding of AUA by isoleucine tRNA on the ribosome. *Nat. Struct. Molec. Biol* 20, 641–643 (2013). [PubMed: 23542153]
33. Bjork GR et al. A primordial tRNA modification required for the evolution of life? *EMBO J* 20, 231–239 (2001). [PubMed: 11226173]
34. Masuda I et al. Loss of N(1)-methylation of G37 in tRNA induces ribosome stalling and reprograms gene expression. *eLife* 10, 70619 (2021).
35. Muto H & Ito K Peptidyl-prolyl-tRNA at the ribosomal P-site reacts poorly with puromycin. *Biochem. Biophys. Res. Commun* 366, 1043–1047 (2008). [PubMed: 18155161]
36. Wohlgemuth I, Brenner S, Beringer M & Rodnina MV Modulation of the rate of peptidyl transfer on the ribosome by the nature of substrates. *J. Biol. Chem* 283, 32229–32235 (2008). [PubMed: 18809677]
37. Ude S et al. Translation elongation factor EF-P alleviates ribosome stalling at polyproline stretches. *Science* 339, 82–85 (2013). [PubMed: 23239623]
38. Doerfel LK et al. EF-P is essential for rapid synthesis of proteins containing consecutive proline residues. *Science* 339, 85–88 (2013). [PubMed: 23239624]
39. Woolstenhulme CJ et al. Nascent peptides that block protein synthesis in bacteria. *Proc. Natl. Acad. Sci. USA* 110, E878–887 (2013). [PubMed: 23431150]
40. Rajkovic A et al. Translation control of swarming proficiency in *Bacillus subtilis* by 5-amino-pentanolyated Elongation Factor P. *J Biol Chem* 291, 10976–10985, (2016). [PubMed: 27002156]
41. Beckert B et al. Structural and mechanistic basis for translation inhibition by macrolide and ketolide antibiotics. *Nat. Commun* 12, 4466 (2021). [PubMed: 34294725]
42. Pelechano V & Alepuz P eIF5A facilitates translation termination globally and promotes the elongation of many non polyproline-specific tripeptide sequences. *Nucleic Acids Res* 45, 7326–7338 (2017). [PubMed: 28549188]
43. Chadani Y et al. Intrinsic Ribosome Destabilization Underlies Translation and Provides an Organism with a Strategy of Environmental Sensing. *Mol. Cell* 68, 528–539 (2017). [PubMed: 29100053]
44. Chadani Y et al. Nascent polypeptide within the exit tunnel stabilizes the ribosome to counteract risky translation. *EMBO J* 40, e108299 (2021). [PubMed: 34672004]

45. Delsol AA et al. Effect of the growth promoter avilamycin on emergence and persistence of antimicrobial resistance in enteric bacteria in the pig. *J. Appl. Microbiol* 98, 564–571 (2005). [PubMed: 15715858]
46. Gupta P, Sothiselvam S, Vazquez-Laslop N & Mankin AS Deregulation of translation due to post-transcriptional modification of rRNA explains why *erm* genes are inducible. *Nat. Commun* 4, 1984 (2013). [PubMed: 23749080]
47. Gupta P et al. Nascent peptide assists the ribosome in recognizing chemically distinct small molecules. *Nat. Chem. Biol* 12, 153–158 (2016). [PubMed: 26727240]
48. Marks J, Kannan K, Roncase EJ, Klepacki D, Kefi A, Orelle C, Vázquez-Laslop N, Mankin AS Context-specific inhibition of translation by ribosomal antibiotics targeting the peptidyl transferase center. *Proc Natl Acad Sci USA* 113, 12150–12155 (2016). [PubMed: 27791002]
49. Orelle C et al. Identifying the targets of aminoacyl-tRNA synthetase inhibitors by primer extension inhibition. *Nucleic acids research* 41, e144 (2013). [PubMed: 23761439]
50. Becker AH, Oh E, Weissman JS, Kramer G & Bukau B Selective ribosome profiling as a tool for studying the interaction of chaperones and targeting factors with nascent polypeptide chains and ribosomes. *Nat. Prot* 8, 2212–2239 (2013).
51. McGlincy NJ & Ingolia NT Transcriptome-wide measurement of translation by ribosome profiling. *Methods* 126, 112–129 (2017). [PubMed: 28579404]
52. Mangano K et al. Genome-wide effects of the antimicrobial peptide apidaecin on translation termination in bacteria. *eLife* 9, 62655 (2020). Mohammad F, Green R & Buskirk AR A systematically-revised ribosome profiling method for bacteria reveals pauses at single-codon resolution. *eLife* 8, 42591 (2019).
53. Aleksashin NA et al. Assembly and functionality of the ribosome with tethered subunits. *Nat. Commun* 10, 930 (2019). [PubMed: 30804338]
54. Saha CK, Sanches Pires R, Brolin H, Delannoy M & Atkinson GC FlaGs and webFlaGs: discovering novel biology through the analysis of gene neighbourhood conservation. *Bioinformatics* 37, 1312–1314 (2021). [PubMed: 32956448]
55. Katoh K & Standley DM MAFFT multiple sequence alignment software version 7: improvements in performance and usability. *Mol. Biol. Evol* 30, 772–780 (2013). [PubMed: 23329690]
56. Capella-Gutierrez S, Silla-Martinez JM & Gabaldon T trimAl: a tool for automated alignment trimming in large-scale phylogenetic analyses. *Bioinformatics* 25, 1972–1973 (2009). [PubMed: 19505945]
57. Miller MA, Pfeiffer W, Schwartz T Proceedings of the TeraGrid Conference: extreme digital discovery 1–8 (2011).
58. Minh BQ et al. IQ-TREE 2: new models and efficient methods for phylogenetic inference in the genomic era. *Mol. Biol. Evol* 37, 1530–1534 (2020). [PubMed: 32011700]
59. Larsson A AliView: a fast and lightweight alignment viewer and editor for large datasets. *Bioinformatics* 30, 3276–3278 (2014). [PubMed: 25095880]
60. Krishnamoorthy G et al. Breaking the permeability barrier of *Escherichia coli* by controlled hyperporination of the outer membrane. *Antimicrob. Agents Chemother* 60, 7372–7381 (2016). [PubMed: 27697764]

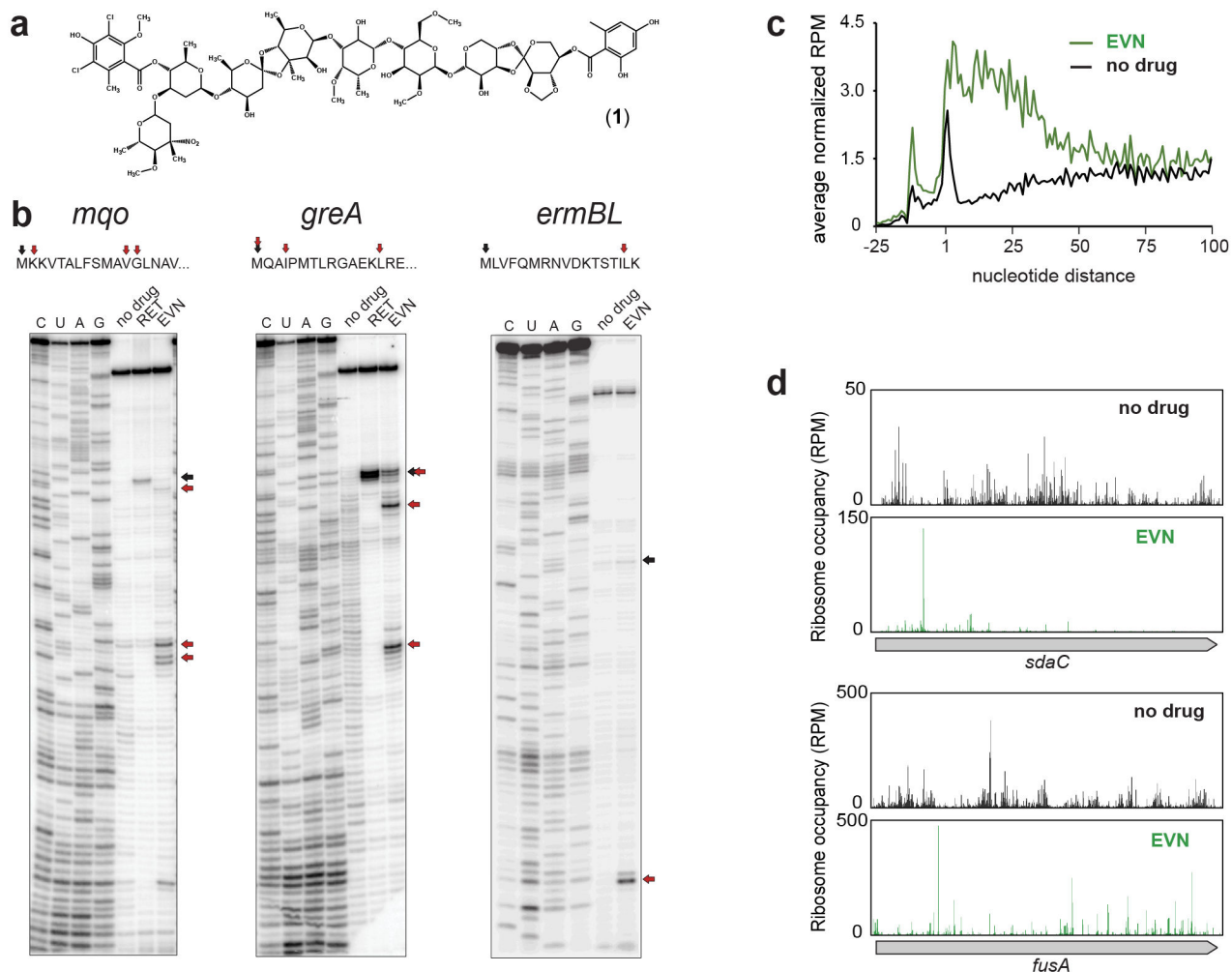


Figure 1: Evernimicin mainly inhibits translation elongation in vitro and in vivo.

a, Chemical structure of EVN. **b**, Mapping by toeprinting the sites of EVN-induced ribosome stalling during in vitro translation of different mRNA ORFs during in vitro translation. Selection of the model genes for in vitro experiments was based on the results of Ribo-seq analysis (*mgo* and *greA*) or previous reports (*ermBL*)¹³ Shown are representative gels from at least two independent experiments. Black arrows indicate ribosomes arrested at the start codons of the ORFs by the translation initiation inhibitor retapamulin (RET)²⁰. Red arrows show the stalling sites of EVN-arrested ribosomes. **c**, Metagenesis plots representing the distribution of ribosomes in the vicinity of start codons of actively translated genes in control cells (black) or cells treated with EVN (green). Included in the analysis were genes (n=1083) separated from the nearest upstream gene by >50 nucleotides. The nature of the ribosome density peak upstream from the start codon is unclear. **d**, Examples of individual genes where EVN causes general redistribution of translating ribosomes and ribosome accumulation at single (top) or multiple (bottom) sites within the ORF. Distribution of rfp along in the same genes in untreated cells is shown for comparison. See also Extended Data Fig. 4.

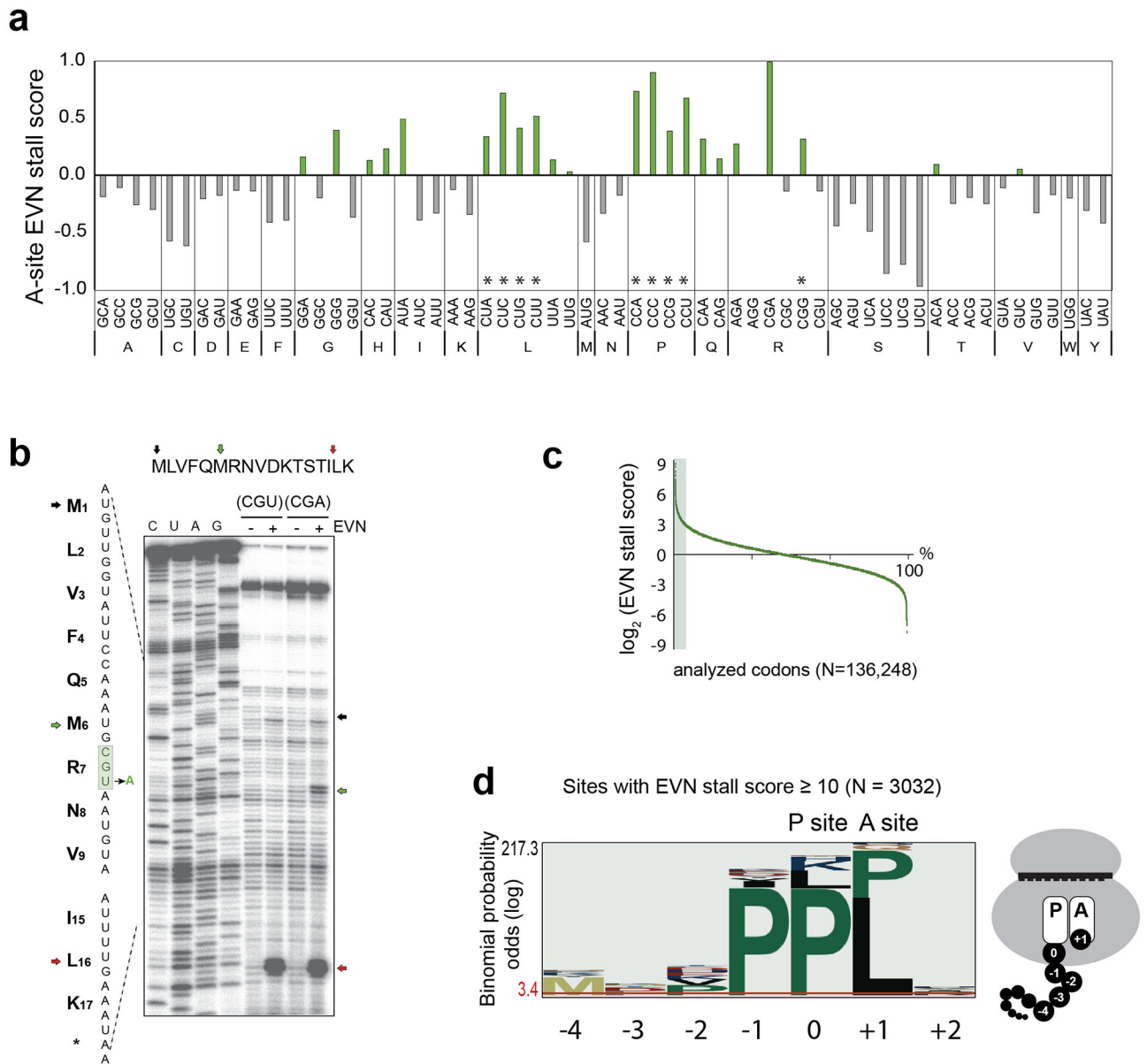


Figure 2: Specific features of the sites of EVN-induced translation arrest

a, The genome-wide EVN stall scores (calculated as normalized codon occupancy in EVN-treated sample relative to that in the untreated control) for each of the codons in the ribosomal A site. The codons marked with an asterisk (*) are decoded by tRNAs whose G37 residue is methylated by TrmD^{33,34}. **b**, Toeprinting analysis of EVN-mediated ribosome stalling during translation of the *emBL* ORF carrying the wt Arg₇ codon CGU or with the same codon mutated to CGA. Black arrow indicates the position of a toeprint band representing ribosome stalled at the start codon, red arrow shows the ribosomes stalled at the Leu₁₆-UUG codon (also shown in Fig. 1a). The green arrow marks the band representing the EVN-arrested ribosomes with the mutagenized Arg₇-CGA codon in the A site. Sequencing reactions lanes are labeled as C, U, A, G. Shown is one representative gel of the two independent experiments. **c**, Plot of the EVN-stall scores of the analyzed codons genome-

wide. The sites with the stall scores ≥ 10 (3032 sites out of 136,248 analyzed) are shaded. **d**, pLogo analysis of the amino acids encoded at the sites of strongest EVN action (shaded area in panel c). The codon occupying the ribosomal P site was set as "0". The cartoon shows schematically the relative positions of the analyzed amino acid residues in the translating ribosome.

Author Manuscript

Author Manuscript

Author Manuscript

Author Manuscript

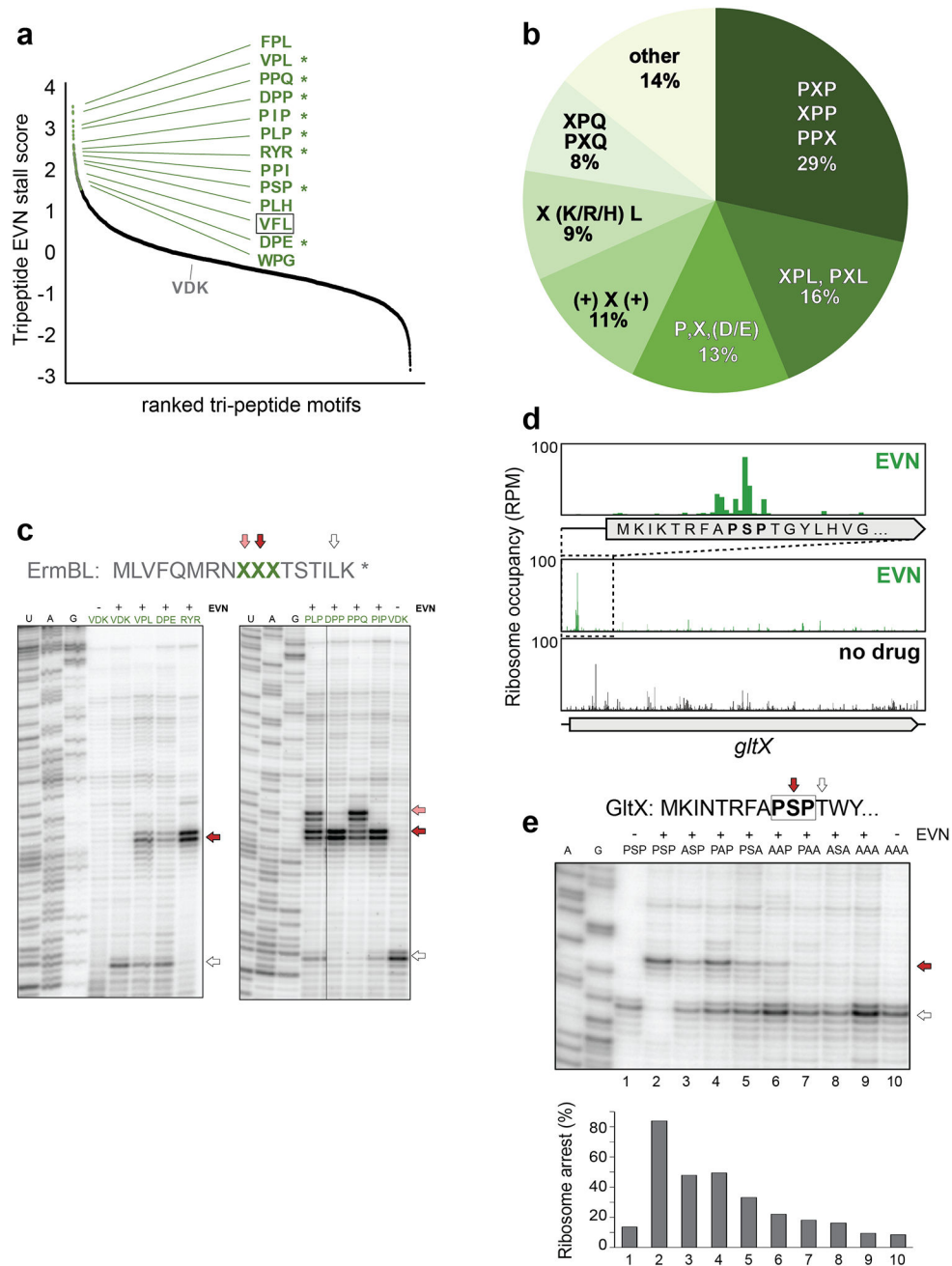


Figure 3: EVN arrests ribosomes at sites encoding specific tripeptide motifs

a, Plot of EVN stall scores for tripeptides motifs. Tripeptides with stall score ≥ 2 SD from the mean of all motifs are indicated with green dots. Representative tripeptide sequences are shown. Sequences tested in toeprinting experiments (panels c and e) are marked by asterisks. The tripeptide sequence VFL, which is found in the EmtAL leader peptide (see Fig. 4), is boxed. Ranking placement of the non-stalling VDK peptide that was mutated in the *ermBL* template (panel c) is indicated. **b**, Relative occurrence of the most prevalent tripeptide motifs at the sites of strongest EVN action ($n = 98$). **c**, In vitro toeprinting for ribosome stalling on *ermBL* templates where the segment encoding the original Val₉Asp₁₀Lys₁₁ sequence

of the ORF was swapped with sequences encoding specific EVN-arrest tripeptide motifs (among those shown in panels **a** and **b**). Translation arrest by EVN at the introduced sites are indicated with red and pink arrows. The white arrow shows the ribosomes that, after escaping arrest at the introduced tripeptide motifs, stall at Leu₁₆-UUG codon of *ermBL* (see Fig. 1a). Lanes corresponding to samples containing no antibiotic are labeled with “-”. Sequencing reactions lanes are labeled as U, A, G. **d**, Ribosomal density profile of the *gltX* gene in control or EVN treated cells. The inset shows EVN-mediated of ribosome accumulation at the early *gltXPXP* motif Pro₈Ser₉Pro₁₀. **e**, Toeprinting analysis of EVN-mediated arrest at the modified *gltX* template (see Extended Data Fig. 6a) with the original or mutated Pro₈Ser₉Pro₁₀ motif. Red arrow indicates ribosomes with EVN stalled at codon 10. Ribosomes that escape EVN arrest become stalled at Thr₁₂ codon (white arrow) preceding the introduced Trp₁₃ codon, because reactions are depleted from Trp-tRNA by the addition of the Trp-RS inhibitor indolmycin. Lanes of samples with no EVN are marked with “-”. Sequencing reactions lanes are labeled as A, G. Toeprinting analysis of ribosome stalling by EVN at the unmodified *gltX* template is shown in Extended Data Fig 6a. Representative gels from at least two independent experiments are shown in panels **c** and **e**.

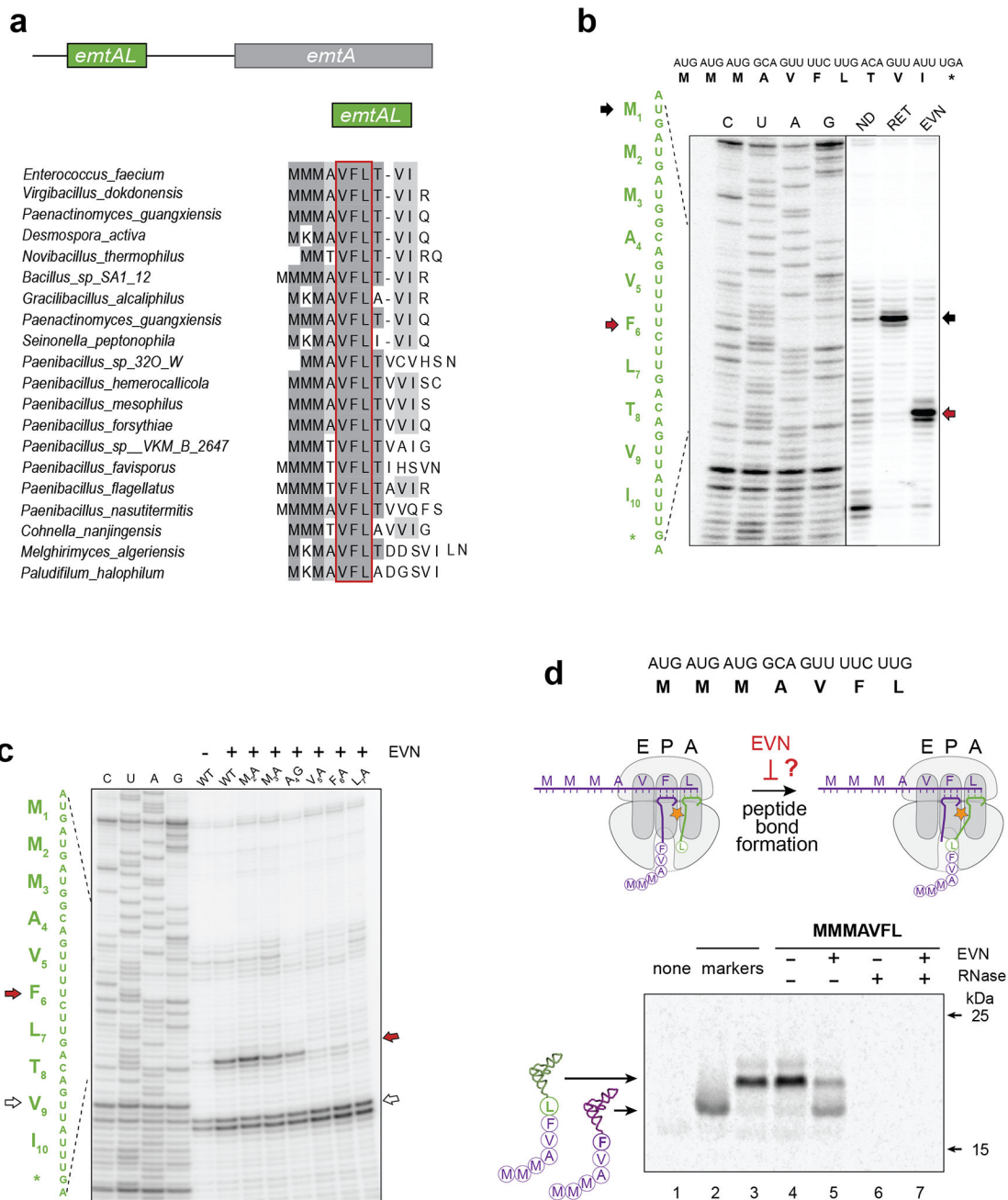


Figure 4: Programmed EVN-mediated translation arrest may control expression of orthosomycin-resistance genes.

a, A conserved leader small ORF (that we named *emtAL*) precedes the orthosomycin-resistance gene *emtA*. The amino acid sequences encoded by *emtAL* ORFs of different bacterial species is shown. The VFL sequence (boxed in red) present in all the identified *emtAL* leader ORFs, is one of the tripeptide motifs associated with the strongest EVN arrest sites (see Fig. 3 a–b). **b**, Toeprinting analysis of ribosome arrest induced by EVN during in vitro translation of the *emtAL* ORF of *Enterococcus faecium*. Inclusion of the initiation inhibitor retapamulin²⁰ (sample labeled RET) helped identified the first of the three consecutive AUG codons as the start codon of the ORF (marked with black arrows).

Red arrows indicate ribosomes stalled by EVN at the Phe₆ codon of the *emtAL* VFL sequence. **c**, Toeprinting analysis of EVN-mediated ribosome stalling in mutant *emtAL* ORF where codons 2–7 of the wt *emtAL* were individually substituted by Ala or Gly codons. Red arrow indicates ribosomes stalled by EVN at codon Phe₆ of the ORFs. White arrow shows ribosomes trapped at Val₉ codon because reactions lacked Ile-tRNA due to the presence of Ile-RS inhibitor mupirocin. Sequencing reactions are shown. **d**, Testing whether EVN inhibits peptide bond formation. Top: sequence of the truncated *emtAL* template, encoding the MMMAVFL peptide and lacking a stop codon, used in the experiment. Middle: cartoon representation of the experimental scheme. Inhibition of peptide bond formation by EVN would lead to the appearance of MMMAVF-tRNA^{Phe}. Bottom: Gel electrophoresis of the in vitro translation products. Reactions contained [¹⁴C]-Phe and were carried without or with EVN (500 µg/mL). Reaction on lane 1 ('none') contained no template. Mobility markers (lanes 2 and 3) were prepared by translating non-stop templates encoding the MMMAVF or MMMAVFL peptides. Samples in lanes 6 and 7 were treated with RNase I; the resulting small peptides (MMMAVF and MMMAVFL) are not retained in the gel. Electrophoretic mobility of molecular weight protein markers (of 25 and 15 kDa) is indicated. The Coomassie-stained gel is shown in the Source Data file. Representative gels from at least two independent experiments are shown in panels **b**, **c** and **d**.

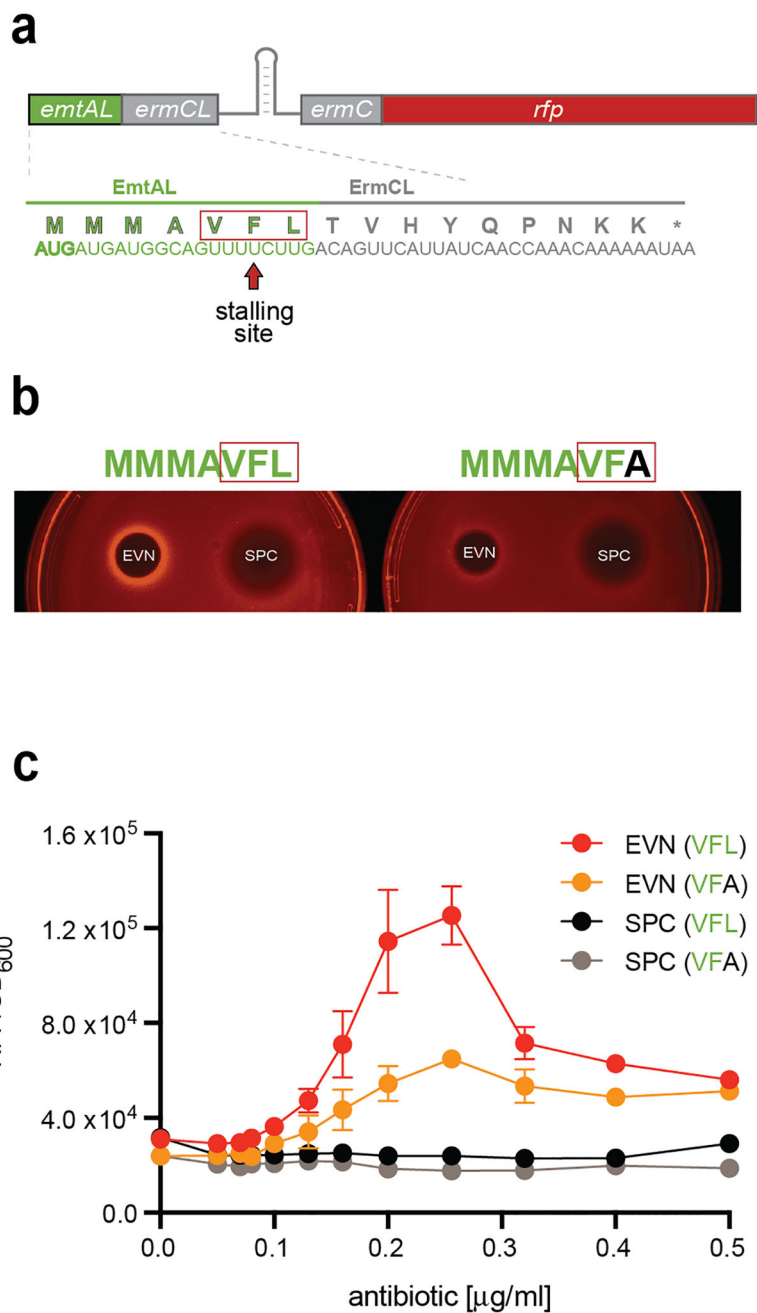


Figure 5. EVN arrests the ribosome translating the EmtAL peptide in vivo

a, Schematics of the *emtAL-ermCL-ermC-rfp* reporter for testing EVN-dependent translation arrest within the *emtAL* leader ORF VFL sequence. In the wt *ermCL-ermC* operon, macrolide dependent ribosome stalling at the 9th codon of *ermCL* leads to activation of *ermC* expression^{25,47}. In the shown construct, the first 10 *ermCL* codons were replaced with 7 codons of *emtAL* to render reporter activation by ribosome stalling at the Phe₆ codon. The reporter expression is monitored following fluorescence of the RFP protein, whose gene, lacking its own start codon, is fused in frame after the first four codons of *ermC*. The nucleotide sequences of the hybrid *emtAL-ermCL* leader ORF and the encoded protein

are shown. The EVN stalling motif VFL of EmtAL is boxed in red. **b**, Drop-diffusion test demonstrating activation of the reporter expression due to EVN-dependent ribosome stalling. A drop of antibiotic solution was placed on agar plates inoculated with *E. coli* cells carrying the reporter cassette. Diffusion generates an antibiotic concentration gradient preventing cell growth near the site of application (black area). Farther away from the drop, subinhibitory concentrations of EVN (but not of the non-inducing control antibiotic spectinomycin, SPC) activate the reporter expression (*left*). Changing the EmtAL's VFL motif to VFA diminishes the EVN-mediated induction of RFP expression (*right*). **c**, Induction of the reporter expression monitored in liquid culture in cells grown at varying concentrations of EVN or SPC. The dots on the plot represent the average experimental values between three biological replicates with the error bars indicating s.e.m.

Author Manuscript

Author Manuscript

Author Manuscript

Author Manuscript

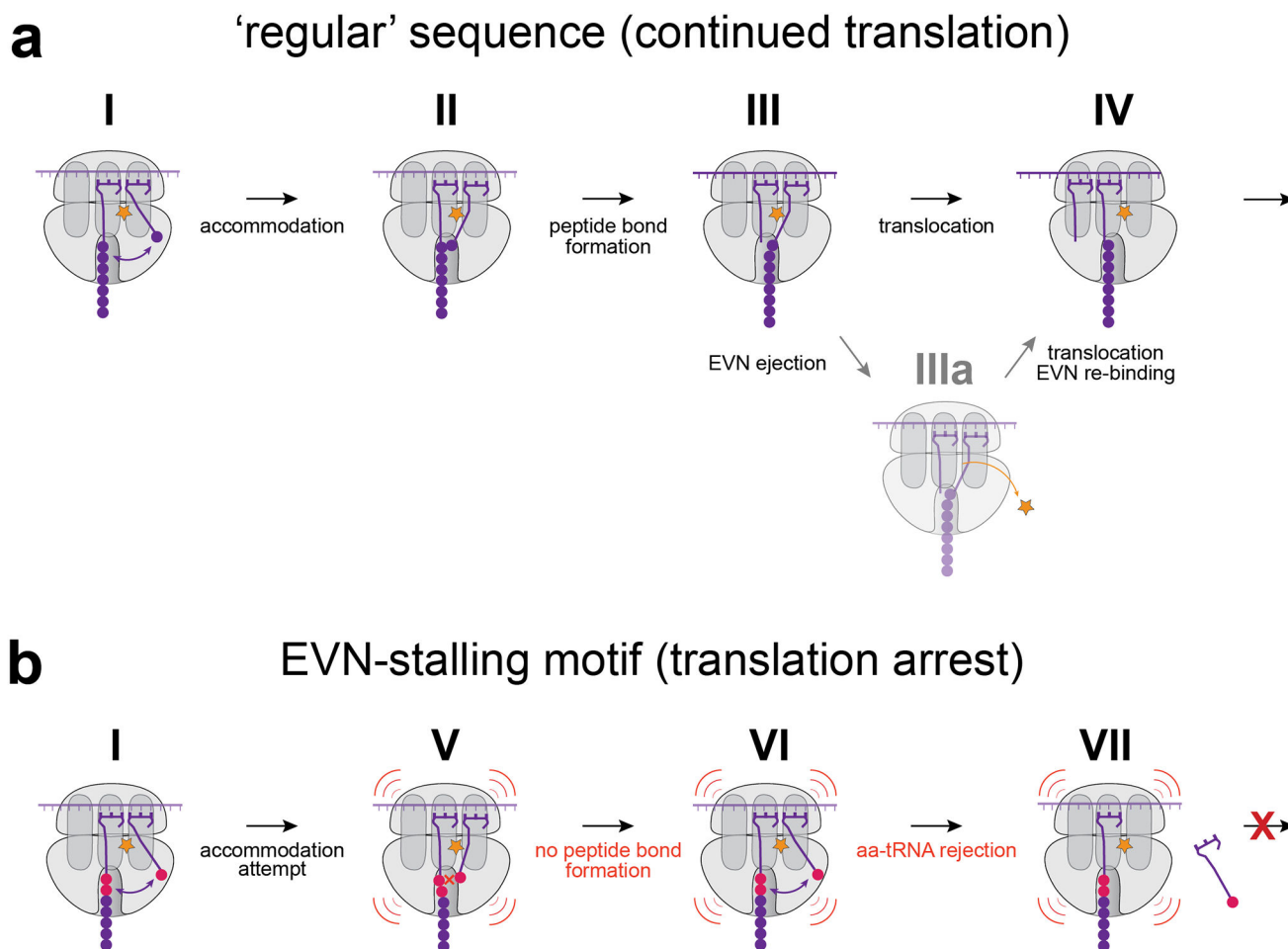


Figure 6: The model of context-specific EVN action.

a, EVN allows for only brief accommodation of the acceptor end of aa-tRNA in the PTC (I and II). With the proper combination of the donor and acceptor substrates, peptide bond is formed during a short visit of aa-tRNA in the PTC active site and nascent peptide is transferred to the A-site tRNA (III). Translocation may possibly proceed without the antibiotic displacement (IV) or may require temporal ejection of the drug molecule (IIIa), followed by new rounds of translation. **b**, When the ribosome translates the EVN arrest motif, peptide bond formation is not fast enough to transfer peptidyl-residue to the A-site tRNA during its brief excursion into the PTC active site (V, VI). With the weak codon-anticodon interactions in the A-site the incoming aa-tRNA is rejected after few futile attempts (VII) resulting in pronounced ribosome stalling.